Mineral Petrol (2008) 93: 1–46
DOI 10.1007/s00710-007-0217-1
Printed in The Netherlands

Mineralogy and Petrology

Petrological evidence for crustal melting, unmixing, and undercooling in an alkali-calcic, high-level intrusion: the late Sveconorwegian Vinga intrusion, SW Sweden

H. Årebäck[1], **U. B. Andersson**[2], **J. Petersson**[1,*]

[1] Earth Sciences Centre, Department of Geology, Göteborg University, Göteborg, Sweden
[2] Swedish Museum of Natural History, Research Department, Stockholm, Sweden

Received March 1 2007; Accepted October 8 2007; Published online December 6 2007

Editorial handling: R. Milke

Summary

The subvolcanic Vinga intrusion is a quartz jotunite to monzogranite located in the outermost part of the Göteborg archipelago, SW Sweden. It is one of a number of post-kinematic, late Sveconorwegian intrusions in the region. Rocks in the intrusion display complex, but well preserved igneous textures, including complexly zoned plagioclase megacrysts (cellular) and skeletal/acicular crystals of apatite, zircon, ilmenite and pyrite. The intrusion has high contents of Σ Fe, Ti, P, K, F and high field strength elements, and contains abundant and diverse enclaves (xenolithic, restitic and co-mingled). The cellular plagioclase may represent partially melted and re-equilibrated restitic plagioclase. The skeletal crystals formed due to undercooling and rapid crystallisation in the magma when it was brought to upper crustal levels. Ion-microprobe analyses of skeletal zircons from the intrusion yield a *concordia age* of 951 ± 7 Ma. The protolith of the parental magma is inferred to have been intermediate, meta-igneous and was partially molten under high temperature conditions as revealed from pyroxene thermometry (>1000 °C) on restitic pyroxenes. Miarolitic cavities, in combination with pressure estimates of ≤2 kbar from Al-in-hornblende barometry, indicate an epizonal emplacement depth at final crystallisation temperatures of around 750–800 °C. Zircon

* Present address: Vattenfall Power Consultant AB, Box 475, SE-401 27 Göteborg, Sweden
Correspondence: Present address: H. Årebäck, Boliden Mineral AB, SE-936 81 Boliden, Sweden
e-mail: hans.areback@boliden.com.

saturation occurred late, during rapid cooling below 900 °C, resulting in skeletal morphologies. The magma evolution started with early separation of restitic pyroxenes, plagioclase and Fe–Ti oxides at midcrustal depths, followed by fractionation. The heat source of melting was related to mafic underplating. Evolved parts of this mafic magma were co-mingled with the Vinga magma.

Introduction

The interpretation of textures in igneous rocks is critical for the reconstruction of processes that operated in magmatic systems. Studies that describe and interpret textural and chemical features in intermediate suites of AMCG (anorthosite-mangerite-charnockite-granite) complexes (e.g. Emslie and Hunt, 1990; Emslie, 1991) in terms of mixing or unmixing processes are few. This study intends to rectify this deficit. Within the porphyritic Vinga intrusion in SW Sweden numerous textural disequilibrium features (e.g. skeletal and cellular minerals) have been preserved as a result of shallow level emplacement. This makes it ideally suited for the combined investigation of textures and composition.

Two-pyroxene-bearing granites and syenitoids are commonly associated with Proterozoic massif-type anorthosites and related mafic rocks (e.g. Emslie, 1978; Markl et al., 1998; Duchesne and Wilmart, 1997; Frost et al., 2002; Rämö and Haapala, 1995). Mafic to intermediate rocks in these complexes are commonly represented by cumulate-enriched rocks and jotunites (the term includes e.g. ferrodiorites, monzonorites and monzogabbros). The origin of jotunites has been debated and proposals for their origin include: i) residual magmas after crystallisation of anorthosite from mantle-derived magma (e.g. Emslie et al., 1994; Mitchell et al., 1996; Markl, 2001; Scoates and Chamberlain, 2003), and ii) derivation from melting of lower crustal mafic sources (e.g. Duchesne et al., 1989; Longhi et al., 1999). Regarding the latter mechanism, associated granitoid magmas are considered to be derived by differentiation from jotunitic or related gabbronoritic magmas (e.g. Anderson et al., 2003, Bolle et al., 2003; Vander Auwera et al., 2003). The AMCG two-pyroxene granitoids and syenitoids commonly show mineral assemblages and bulk compositions indicating high (900–1000 °C) crystallisation temperatures (e.g. Kolker and Lindsley, 1989; Anderson et al., 2003). The coeval, bimodal character of the magmas in these suites has commonly resulted in mingled and mixed rocks (e.g. Kolker and Lindsley, 1989; Wiebe, 1980; Eklund et al., 1994).

Origins for such bimodal suites with linear compositional trends in Harker diagrams and containing abundant enclaves of variable types can be summarized into two main hypotheses: i) *magma mixing* between two magmas of contrasting composition, where one is typically more mafic (mantle-derived) than the other, which is felsic and typically crustal (e.g. Blake et al., 1965; Whalen and Currie, 1984; Frost and Mahood, 1987; Bateman, 1995; Sandeman et al., 2000), and ii) *restite unmixing* where the gradual separation of solid source residue (restite material) from the melt fraction yields the chemical variation (e.g. White and Chappell, 1977; Chappell et al., 1987; Chen et al., 1990).

Mafic microgranular (or magmatic) enclaves (MMEs) that form by ‘quenching’ of high-temperature mafic, or partly hybridized, magma droplets in cooler more silicic magma (mingling) (e.g. Wager and Bailey, 1953; Walker and Skelhorn,

1966; Vernon, 1984; Ratajeski et al., 2001) are typical for rock suites formed by mixing of contrasted magmas (e.g. Lindberg and Eklund, 1988; Larsen and Smith, 1990; Poli and Tommasini, 1991; Altherr et al., 1999; Collins et al., 2000). They are characterised by a magmatic mineralogy, finer grain size than the surrounding host, occasionally chilled margins, and quench textures (Wyllie et al., 1962; Reid et al., 1983; Vernon, 1990; Andersson and Eklund, 1994). MMEs may occur together with restitic enclaves in the same host rock (e.g. Zeck, 1992; Stimac et al., 1995; Hraško et al., 1998).

Disequilibrium mineral textures can result from changes in composition (e.g. as a result of magma mixing; e.g. Hibbard, 1981, 1995; Barbarin, 1990; Halsor and Rose, 1991; Müller and Seltmann, 2002) or from changes in physical conditions (P, T, P_{H_2O}) of a rock system (e.g. Vance, 1965; Lofgren, 1980; Årebäck and Stigh, 1997; Petcovic and Grunder, 2003; Stewart and Pearce, 2004). Such environmental changes may cause rapid 'skeletal' crystallisation due to supersaturation, or conversely (partial) dissolution of crystalline material in undersaturated system, depending on the relative shift in stability relations (e.g. Hibbard, 1995; Johannes and Holtz, 1996; Nakamura and Shimakita, 1998). A typical texture in disequilibrium systems is the cellular or 'sieve' texture, particularly common for plagioclase (e.g. Tsuchiyama and Takahashi, 1983; Johannes et al., 1994; Stewart and Fowler, 2001). In supersaturated systems, it may develop as a result of mixing (Kuo and Kirkpatrick, 1982; Hibbard, 1995) or decompression and/or volatile loss (Landi et al., 2004). In undersaturated systems, dissolution may result from a temperature increase (Kaczor et al., 1988; Johannes et al., 1994; Petcovic and Grunder, 2003) and/or mixing (Tsuchiyama, 1985; Andersson and Eklund, 1994; Hattori and Sato, 1996), or decompression (Vance, 1965; Nelson and Montana, 1992; Årebäck and Stigh, 1997; Singer et al., 1993).

Geological setting

The Vinga intrusion is a plagioclase porphyritic granite to quartz jotunite intrusion located in the Sveconorwegian (i.e. Grenvillian) orogen (1.2–0.9 Ga) of SW Sweden. Rocks from the intrusion display complex, but well-preserved, igneous textures and crop out on Vinga and a few nearby islands in the outermost part of the Göteborg Archipelago (Fig. 1). Although contacts with the surrounding Mesoproterozoic gneisses are not exposed, internal magmatic structures and exposures indicate that the intrusion is a WNW-ESE-elongated body, at least 4×1 km in size. Lundegårdh (1953) briefly described the Vinga intrusion as a plagioclase-porphyrite, rich in angular xenoliths, while Lundqvist (2000) termed it a quartz monzodiorite, and Åhäll and Schöberg (1999) referred to it as a hybrid, dike-like body, having a monzonitic composition.

The intrusion is one of a large number of post-kinematic rocks that were emplaced in the southwestern part of the Fennoscandian Shield towards the end of the Sveconorwegian orogeny. The majority of these rocks are granites with U–Pb and Pb–Pb dates in the interval 950 to 920 Ma (see Andersen et al., 2002, and references therein). However, the rock group includes some anorthositic and mafic intrusions, such as the 935 ± 3 Ma Göteborg dykes (Hellström et al., 2004), the 916 ± 11 Ma Hakefjorden Complex (Scherstén et al., 2000) and the voluminous

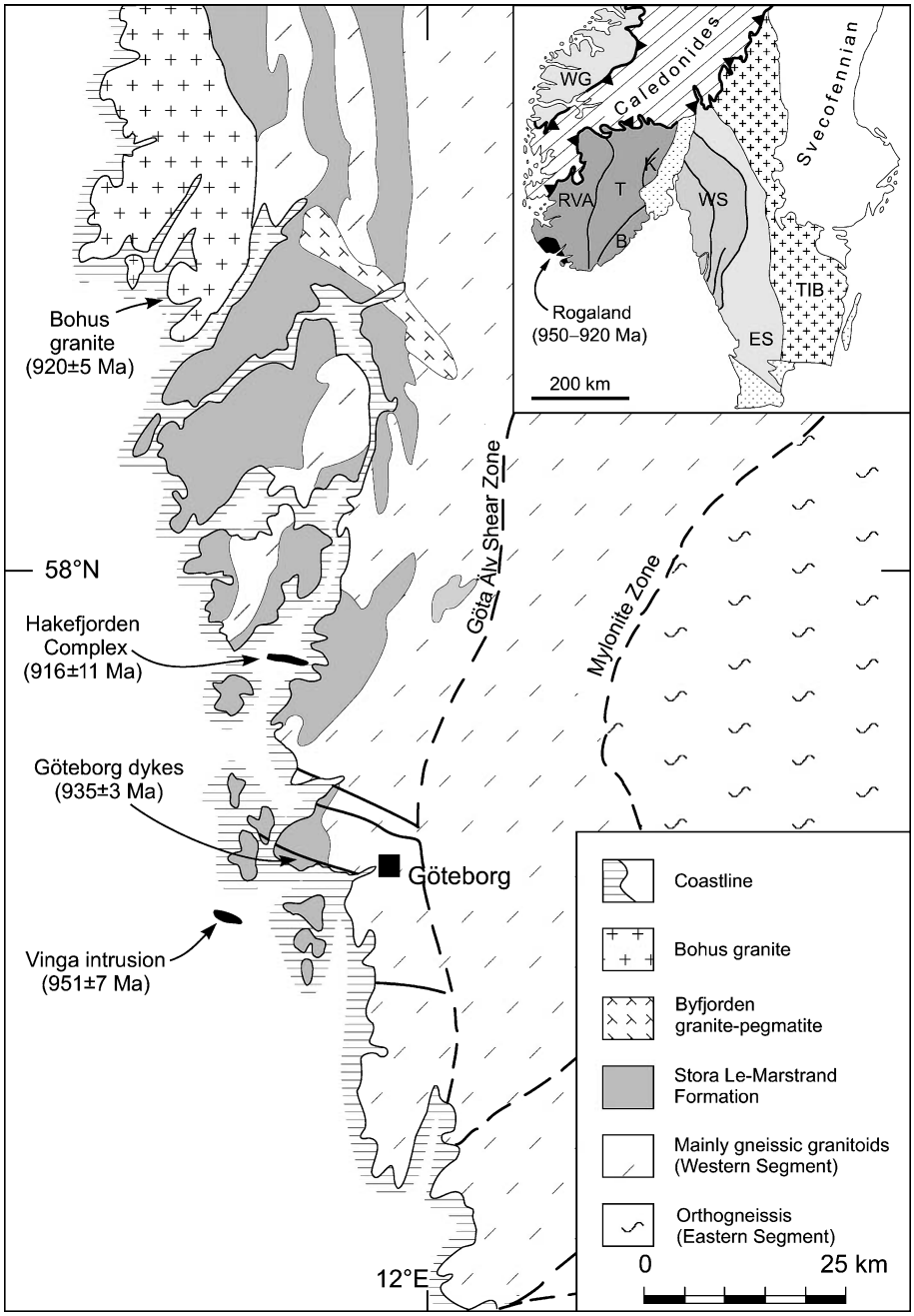

Fig. 1. Generalised geological map of SW Sweden showing the location of the Vinga intrusion and other late Sveconorwegian intrusions in the area. The inset map shows major lithotectonic units of southern Scandinavia. Different shades of grey: Sveconorwegian province. Subdivision of internal allochthonous (dark grey), external allochthonous (medium grey) and external para-autochthonous (light grey) terranes after Romer and Smeds (1996). The most voluminous late Sveconorwegian intrusions occur in the internal allochthonous. RAV: Rogaland-Vest Agder Sector. T: Telemark sector. K: Kongsberg sector. B: Bamble sector. WS: Western Segment. ES: Eastern Segment. WG: Western Gneiss Region. TIB: Trans-Scandinavian Igneous Belt

~950 to 920 Ma Rogaland Igneous Complex (Schärer et al., 1996; Andersen and Griffin, 2004) (Fig. 1).

The region affected by the Sveconorwegian orogeny is a mosaic of crustal blocks separated by shear zones, and the Vinga intrusion occurs within a ca. 20–70 km wide crustal segment, referred to as the Western Segment. Towards the west, this segment is delimited by the Oslo Graben and in the east by the Mylonite Zone (Fig. 1). The main constituents of the segment are polymetamorphic paragneisses and gneissic granitoids with magmatic ages between 1.62 and 1.55 Ma (e.g. Connelly and Åhäll, 1996; Åhäll et al., 1998). The Vinga intrusion has intruded a sequence of migmatized greywacke-type sediments, referred to as the Stora Le-Marstrand (SLM) formation, with a minimum depositional age of 1587 Ma (Åhäll et al., 1998).

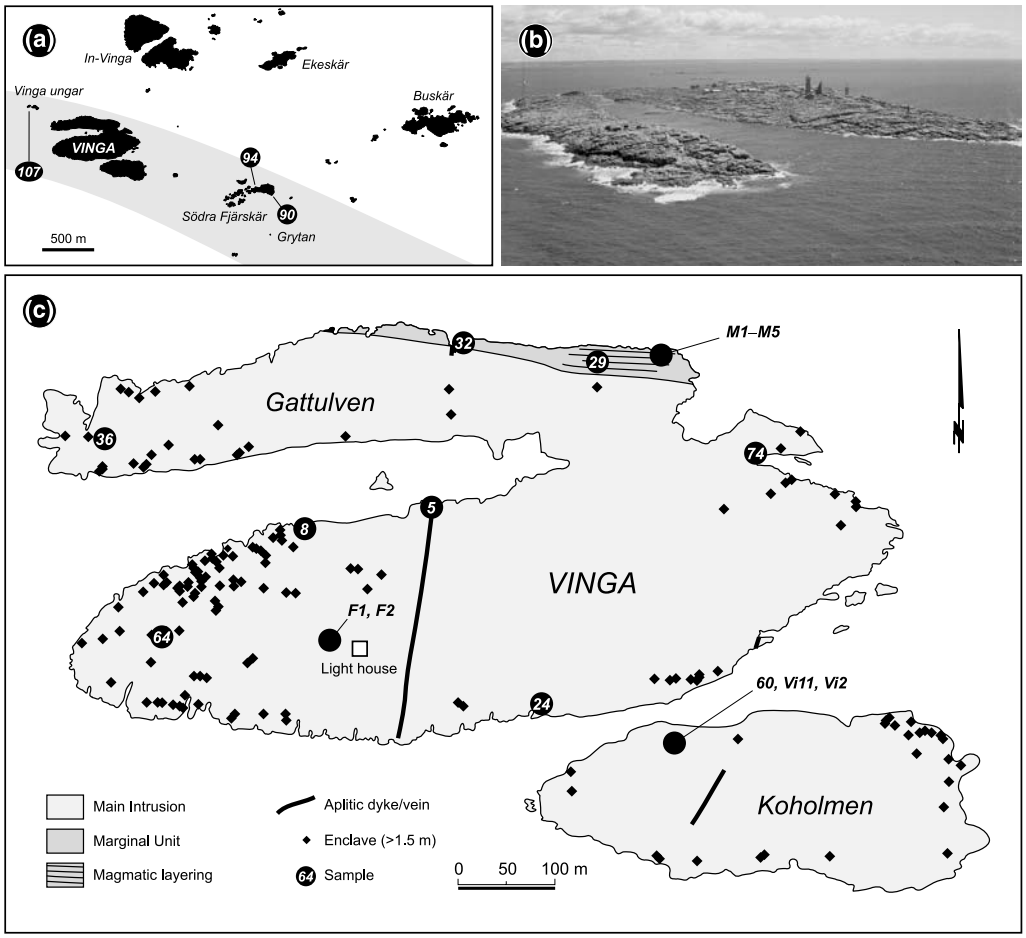

Fig. 2. (**a**) Map of Vinga and the surrounding islands in the outermost part of Göteborg archipelago. The shaded area represents the estimated limit of the Vinga intrusion. Rocks to the north of the shaded area are dominated by gneissic granitoids and paragneisses of the Stora Le-Marstrand Formation. (**b**) Aerial photograph of Vinga Island with the Vinga lighthouse, looking ESE. Photo (by Lars Ericsson) reproduced with the permission of DET AB, Partille, Sweden. (**c**) Geological map of the Vinga intrusion on Vinga and Koholmen islands

Table 1. *Modal composition (vol%) of rocks from the Vinga intrusion*

Rock type	Main Intrusion								Marginal Unit							MME[a]	Aplitic dyke	Granitic seg.
Colour	Grey					Reddish grey												
Sample no.	8	36	60	64	107	74	90	94	M1	M2	M3	M4	M5	29	32	Vi11	5	24
Plagioclase	17.8	18.1	20.3	16.6	16.5	15.4	10.2	10.8	36.9	34.0	40.3	28.6	38.8	30.2	22.7	40	26.9[b]	14.5[b]
Clouded plag.	13.4	18.2	11.9	16.2	19.4	11.9	16.3	14.7	8.7	10.9	9.4	10.0	5.3	4.9	13.2	–	–	–
K-feldspar	21.1	17.4	20.6	22.3	21.6	31.1	28.3	31.8	17.1	15.4	20.4	21.3	18.5	19.2	18.9	10	28.4	50.6
Quartz	17.9	16.6	17.3	20.8	18.3	19.6	18.1	22.5	10.6	10.5	8.8	14.9	9.6	14.9	16.1	1	36.4	25.2
Hornblende	11.2	14.8	14.1	12.6	12.5	9.8	17.3	12.5	5.9	7.1	5.4	6.0	6.9	8.4	12.7	2	–	0.5
Biotite	2.0	1.3	3.6	1.5	2.3	1.2	0.1	0.8	4.3	3.9	1.9	3.4	4.5	4.8	4.9	2	–	0.1
Clinopyroxene	1.6	0.7	1.4	0.4	1.1	0.2	0.5	0.2	2.3	2.1	3.2	3.2	2.6	3.4	1.8	20	–	–
Orthopyroxene	–	–	–	–	–	–	–	–	6.9	8.2	5.2	5.3	6.0	4.1	0.8	10	–	–
Chlorite	9.5	8.3	6.6	5.7	3.6	5.8	4.9	3.4	1.2	1.3	0.5	1.6	0.7	3.0	2.0	–	5.5	6.4
Fe–Ti oxides	4.1	3.4	2.8	2.7	2.3	3.1	3.4	2.5	4.2	4.3	3.5	4.2	5.7	4.7	5.0	14	0.7[c]	1.5
Apatite	1.1	0.8	1.0	1.1	1.3	1.0	0.7	0.6	1.6	1.7	1.3	1.2	1.1	2.3	1.7	1	0.4	0.2
Other[*]	0.3	0.4	0.4	0.1	1.1	0.9	0.2	0.2	0.3	0.6	0.1	0.3	0.3	0.1	0.2		1.7	1.0
Total counts	1564	1899	1557	1653	1796	1784	1553	1682	1945	1683	1508	1477	1452	1729	1316		1427	1141

[*] Include zircon, epidot, calcite, allanite, sphene, pyrite, pyrrhotite

[a] Contents are estimated due to difficulties in point counting this fine-grained rock

[b] Plagioclase in the aplitic dyke and the granitic segregation consists of albite

[c] Including hematite and possible pyrite

Samples and methods

Twenty samples were selected for whole-rock geochemistry, to cover all apparent textural and lithological varieties of the Vinga intrusion (Fig. 2). Except for three MME samples (Vi11, F1 and F2), weighing approximately 50 g each, all whole-rock samples exceed 2 kg in weight. They were all crushed in a jaw-crusher and ground in a chrome steel swingmill at the Earth Sciences Centre, Göteborg University. The geochemical analyses were performed by the Centre de Recherches Pétrographiques et Géochimiques (CRPG), France; major elements were determined by ICP-AES and trace elements by ICP-MS. Duplicate analysis of sample F1 and F2 showed that the reproducibility for trace elements is better than 12% for concentrations up to about 4 times the detection limit, and better than 9% for higher concentrations. The reproducibility for the major elements is better than about 2%. Fluorine was analysed in three samples (24, 107, and M2) by ACME Analytical Laboratories, Canada, using the Na_2O fusion method.

A polished thin-section was also prepared for each of the twenty whole-rock samples. All these thin-sections underwent modal analysis (Table 1). Quantitative mineral analyses and element distribution images were obtained at the Department of Earth Sciences, Uppsala University, using a Cameca Camebax SX50. Operating conditions for spot analyses were 20 kV accelerating voltage, 15 nA beam current, 1–10 μm beam diameter, with counting times of 10–25 s (depending on the element); for element distribution images, 20 kV accelerating voltage and 30 nA beam current were used. Calibration was performed on natural and synthetic mineral standards from Cameca. Microtextural studies and mineral identification were performed using a Link energy-dispersive spectrometer system, attached to a Zeiss DSM 940 scanning electron microscope (SEM) at the Earth Sciences Centre, Göteborg University.

Zircons from sample 107 were separated by crushing, sieving, panning and heavy liquids, and were examined using a Zeiss DMS 940 SEM. U–Th–Pb analyses of zircons were made using the CAMECA ims 1270 ion microprobe (NORDSIM facility) at the Swedish Museum of Natural History, Stockholm. The analytical and data reduction procedures are similar to those given by Whitehouse et al. (1997, 1999). Pb/U calibration was made relative to Geostandards zircon 91500 (1065.4 Ma) (Wiedenbeck et al., 1995).

Field relations

The exposed part of the Vinga intrusion extends from ‘Grytan’ islet in the east to ‘Vinga ungar’ islet in the west, over a distance of about 4 km (Fig. 2). Seafloor topography suggests that the intrusion extends WNW for at least 5 additional kilometers (Åhäll and Schöberg, 1999). The rock is plagioclase porphyritic, medium-grained and grey in hand specimen, although reddish grey varieties occur locally. The reddish colour is generally more common towards the ESE and correlates positively with the modal content of K-feldspar.

Rounded, complex plagioclase megacrysts (CPM) are abundant (Fig. 3), as are different types of enclaves, including: i) numerous hornblende-mantled quartz fragments that are evenly distributed throughout the intrusion (Fig. 3a, b), and

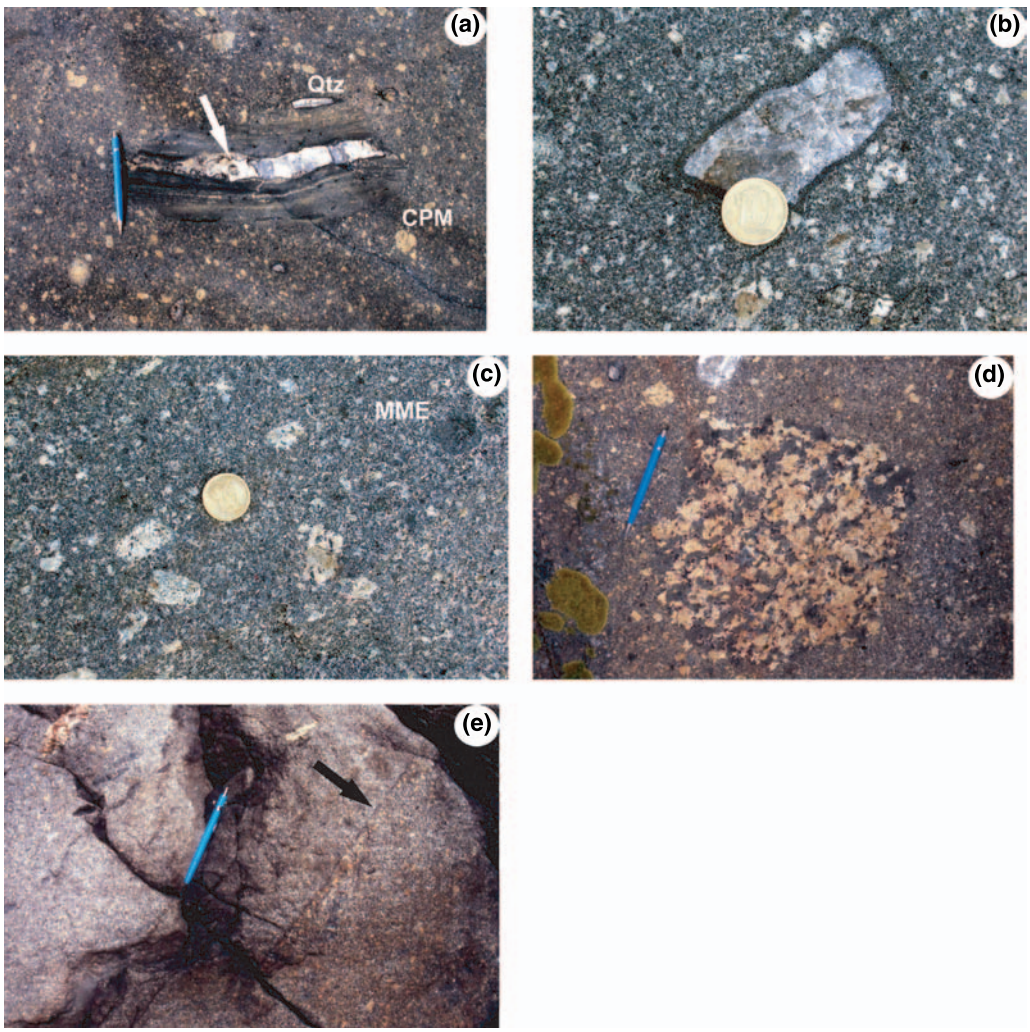

Fig. 3. Photographs of representative field structures in the Vinga intrusion. (**a**) Vinga rock containing rounded, complex plagioclase megacrysts (CPM), a rounded (partly digested) paragneiss xenolith (Stora Le-Marstrand metasediment) and a hornblende-mantled quartz fragment (Qtz). Note the black hornblende mantle (arrow) around the quartz vein in the xenolith. Length of pencil is 14 cm. (**b**) Quartz fragment mantled by a mm-wide rim of hornblende. (**c**) Detail showing dark mafic mineral inclusions in CPM and a rounded mafic microgranular enclave (MME). Diameter of coin is 2.0 cm. (**d**) Feldspar-dominated enclave, consisting of coarse-grained feldspars (light grey, complexly zoned plagioclase and granophyre) and fine-grained mafic minerals (dark). (**e**) Marginal Unit of the Vinga intrusion, showing internal magmatic structures (arrow). View of vertical outcrop is to the east

ii) partly digested gneiss fragments (paragneisses, orthogneisses and a few amphibolites), which are locally common (Fig. 3a). Small rounded mafic microgranular enclaves (MME) and coarse-grained feldspar-dominated enclaves are also important components of the intrusion (Fig. 3c, d). Late stage magmatic features such as miarolitic cavities and granitic segregations are common, as well as a few cross-

cutting N10–30° E trending late magmatic aplitic dykes. Late- to post-magmatic joints at N10° E are common throughout the intrusion. These joints are vertical to subvertical, persistent and lined with peripheral quartz + K-feldspar ± calcite and chlorite ± calcite in their central parts.

The northern side of Vinga Island exposes a slightly more mafic and homogenous variety of the intrusion, with internal planar structures (magmatic layering), containing orthopyroxene in addition to the ubiquitous clinopyroxene, and is here referred to as the 'Marginal Unit' (Fig. 2). This unit contains fewer megacrysts and enclaves than the rest of the intrusion. The internal layers range in width from a few decimetres to about one metre (Fig. 3e). The orientation of the layers varies from N75° W to E–W (i.e. parallel to the length of the intrusion) dipping 50° to 60° towards the south. The contact between the Marginal Unit and the Main Intrusion is rather diffuse, but commonly marked by the parallel alignment of hornblende-mantled quartz fragments.

Petrography

Main Intrusion

The rock matrix consists of plagioclase, K-feldspar, quartz, hornblende, biotite, chlorite, Fe–Ti oxides and relics of clinopyroxene, in order of decreasing abun-

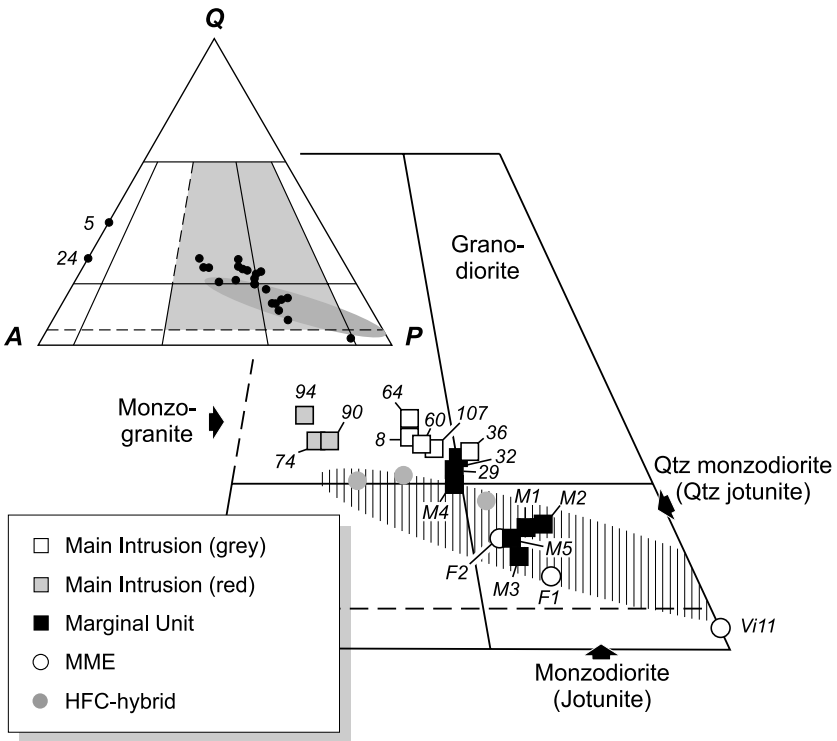

Fig. 4. QAP modal classification diagram after Streckeisen (1976). Rock nomenclature for orthopyroxene-bearing rocks is in brackets. For comparison rocks from the Hakefjorden Complex (HFC) are included (shaded area = HFC norite and monzonorite)

Table 2. *Representative mineral analyses from the Marginal Unit, Main Intrusion and the granitic segregation*

Rock type	Marginal Unit							Main Intrusion					Granitic segregation			
Sample	M1	M1	M1	M1	M1	29	M3	Vi2	Vi2	Vi11	Vi2	Vi11	24	24	24	24
no.	2:5	2:6	2:3	1:1	2:11	4:11	2:1	2:6	2:7	2:4	2:3	2:8	4:5	4:7	4:2	4:9
Mineral	Pl (core)	Pl (rim)	Opx	Cpx	Hbl	Bt	Ilm	Pl (core)	Pl (rim)	Kfs	Hbl	Bt	Pl (albite)	Kfs	Hbl	Ilm
SiO_2 (wt%)	54.35	62.96	52.11	51.21	44.82	36.62	0.02	58.19	62.86	65.13	46.04	35.60	68.54	64.98	44.40	0.00
TiO_2	0.12	0.00	0.53	0.77	1.29	4.05	48.56	0.00	0.01	0.04	1.18	3.52	0.00	0.02	1.14	46.94
Al_2O_3	27.49	22.81	1.59	1.79	6.60	12.35	0.00	25.21	21.66	19.05	5.79	12.39	19.53	18.55	6.66	0.00
FeO	0.56	0.45	20.78	13.73	16.24	22.55	49.43	0.41	0.17	0.08	17.82	26.72	0.01	0.00	25.01	48.59
MnO	0.00	0.00	0.35	0.32	0.21	0.10	0.64	0.00	0.00	0.00	0.20	0.13	0.03	0.03	0.32	1.62
MgO	0.00	0.00	22.91	13.93	12.75	10.51	0.03	0.00	0.01	0.00	12.19	7.36	0.00	0.01	6.78	0.00
CaO	10.42	4.16	1.69	17.60	10.77	0.00	0.00	7.79	4.00	0.57	10.70	0.00	0.25	0.00	10.77	0.13
Na_2O	5.34	9.06	0.00	0.28	1.78	0.15	0.00	7.31	9.11	2.87	2.04	0.00	11.51	0.16	2.04	0.00
K_2O	0.37	1.00	0.00	0.00	1.04	9.21	0.00	0.53	0.38	12.08	1.00	8.99	0.03	16.51	1.18	0.00
Total	98.65	100.44	99.97	99.63	95.50	95.54	98.67	99.44	98.20	99.82	96.98	94.72	99.90	100.26	98.29	97.28
Number of oxygens	8		6		23	24	3	8			23	24	8		23	3
Si	2.491	2.791	1.936	1.940	6.876	6.198	0.001	2.629	2.832	2.975	6.993	6.211	2.995	2.996	6.908	0.000
Ti	0.004	0.000	0.015	0.022	0.149	0.516	0.953	0.000	0.000	0.001	0.135	0.462	0.000	0.001	0.133	0.939
Al	1.485	1.191	0.070	0.080	1.193	2.463	0.000	1.342	1.150	1.025	1.037	2.548	1.006	1.008	1.222	0.000
Fe	0.022	0.017	0.646	0.435	2.084	3.192	1.078	0.015	0.006	0.003	2.264	3.898	0.000	0.000	3.254	1.081
Mn	0.000	0.000	0.011	0.010	0.027	0.014	0.014	0.000	0.000	0.000	0.026	0.019	0.001	0.001	0.042	0.037
Mg	0.000	0.000	1.269	0.786	2.916	2.652	0.001	0.000	0.000	0.000	2.760	1.915	0.000	0.000	1.571	0.000
Ca	0.512	0.197	0.067	0.714	1.769	0.000	0.000	0.377	0.193	0.028	1.742	0.000	0.012	0.000	1.795	0.004
Na	0.475	0.779	0.000	0.021	0.530	0.048	0.000	0.641	0.796	0.254	0.601	0.000	0.975	0.014	0.616	0.000
K	0.022	0.056	0.000	0.000	0.203	1.988	0.000	0.030	0.022	0.704	0.193	2.001	0.002	0.971	0.235	0.000
Σ cations	5.010	5.031	4.014	4.008	15.746	17.073	2.047	5.035	5.001	4.990	15.751	17.053	4.991	4.992	15.774	2.061
An/En	50.8	19.1	63.7	40.4				36.0	19.1	2.8			1.2	0.0		
Ab/Fs	47.1	75.4	32.4	22.3				61.1	78.7	25.7			98.7	1.4		
Or/Wo	2.1	5.5	3.4	36.7				2.9	2.2	71.4			0.2	98.6		
Mg#			66.3	64.4	58.3	45.4					54.9	32.9			32.6	
Xgk							0.00									0.00
Xpy							0.01									0.04
Xilm							0.98									0.96
Hornblende classification name					ferrian-magnesio-hornblende						ferrian-magnesio-hornblende				ferri-tschermakitic-hornblende	

Mol.% An = 100Ca/(Ca + Na + K); Ab = 100Na/(Ca + Na + K); Or = 100K/(Ca + Na + K)
Mol.% En = 100Mg/(Mg + Fe + Mn + Ca); Fs = 100Fe/(Mg + Fe + Mn + Ca); Wo = 100Ca/(Mg + Fe + Mn + Ca); Mg# = 100Mg/(Mg + Fe)
Xgk = Mg; Xpy = Mn; Xilm = 1 − (Xgk + Xpy)
The spreadsheet program PROBE-AMPH (Tindle and Webb, 1994) was used to determine classification names for hornblende

dance (Table 1). In QAP ternary classification diagram (Fig. 4), the Vinga intrusion is classified as quartz monzodiorite (quartz jotunite for orthopyroxene-bearing rocks) to monzogranite.

Euhedral to subhedral plagioclase crystals predominate in the intrusion (26–36 vol%). Feldspars, especially plagioclase, are affected by deuteric sericitisation to a variable extent. Matrix plagioclase from both the Main Intrusion and the Marginal Unit is normally zoned, with andesine core compositions, ranging from $\sim An_{50}$ in the northernmost part of the Marginal Unit to $\sim An_{40}$ in the eastern part of the Main Intrusion (Table 2). The most sodic margins are $An_{19–24}$. K-feldspar (17–32 vol%) occurs in interstices and as thin rims on plagioclase. Quartz (17–23 vol%) is typically interstitial and non-undulose. Granophyric intergrowths are common, especially along grain boundaries and as rims on K-feldspar-mantled matrix plagioclase.

The primary mafic minerals in the Main Intrusion, are hornblende (10–17 vol%), biotite (0.1–4 vol%) and clinopyroxene (0.2–2 vol%). Also chlorite is a major constituent (3–10 vol%), but is a secondary alteration product after the above mentioned mafic phases. The hornblende grains are typically euhedral with rims of increased Fe-content. The most common hornblende types in the Main Intrusion and the Marginal Unit are ferrian magnesio-hornblende (core = Mg# 51–61, rim = Mg# 41–45; Fig. 5a). Aggregates/clots, 1–3 mm in diameter, of

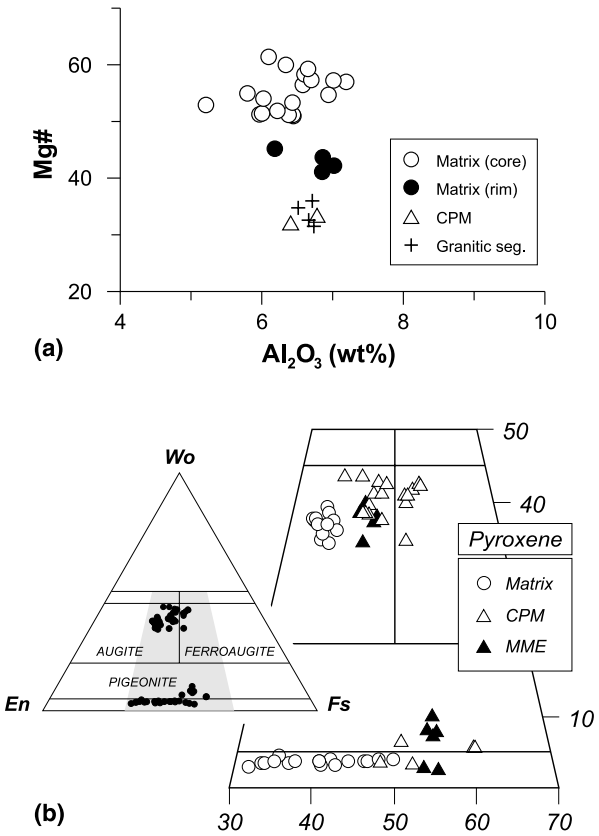

Fig. 5. (**a**) Mg# vs. Al_2O_3 of hornblende from different units of the Vinga intrusion. (**b**) Composition of pyroxenes (and simplified nomenclature) in the Vinga intrusion, plotted in the En-Fs-Wo triangular diagram

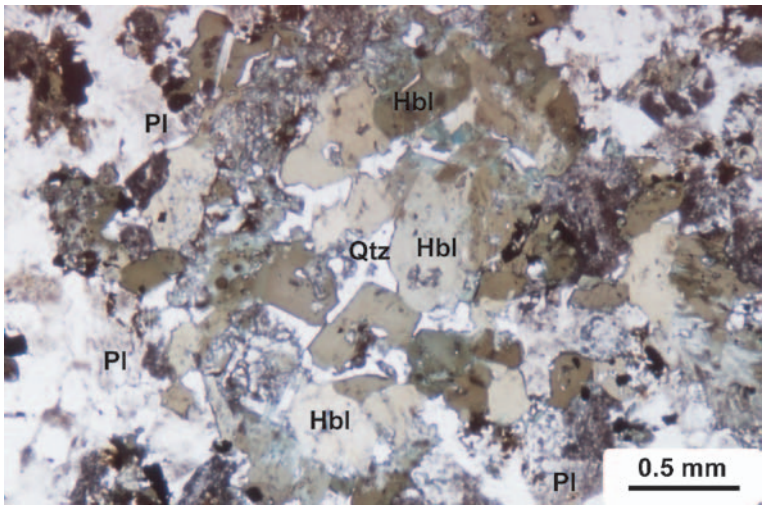

Fig. 6. Photomicrograph of Vinga rock showing aggregate/clot of hornblende (Hbl) with quartz (Qtz) in the central part. Other minerals are mainly plagioclase (Pl; with a varying degree of sericitisation) and minor K-feldspar. Plane-polarised light. Sample 60

euhedral hornblende occur sparsely throughout the rock and are typically intergrown with anhedral quartz in their central parts (Fig. 6). Hornblende also replaces clinopyroxene (Fig. 7b), which rarely occurs as discrete grains. Biotite is typically associated with Fe–Ti oxides and hornblende. Fe–Ti oxides (2–4 vol%) are dominated by ilmenite, although intergrowths of ilmenite and magnetite do occur.

Accessory minerals include apatite (0.5–1 vol%), zircon, epidote, calcite, allanite, sphene, pyrite and pyrrhotite. Skeletal morphologies are observed for zircon, apatite and pyrite. Zircon (Figs. 7a and 11a) typically occurs late in the paragenetic sequence and locally as minute crystals on ilmenite. Apatite occurs as prismatic crystals, but also with acicular and tube-like (hollow) morphologies (Fig. 7c).

Marginal Unit

The Marginal Unit differs from the Main Intrusion by the occurrence of orthopyroxene (1–8 vol%), and by containing slightly more plagioclase, clinopyroxene, Fe–Ti oxides and apatite at the expense of quartz, K-feldspar, hornblende and chlorite. There are fewer megacrysts in the Marginal Unit and their size decreases towards the north where the rock becomes more equigranular. Clinopyroxenes in the Marginal Unit and in the Main Intrusion are augitic ($En_{38-41}Fs_{21-25}Wo_{34-39}$) and orthopyroxene is hypersthene ($En_{48-66}Fs_{31-44}Wo_{3-4}$; Fig. 5b). Normally zoned orthopyroxene is common; the core and rim composition in one grain is $En_{61}Fs_{35}Wo_3$ and $En_{45}Fs_{50}Wo_4$, respectively. Orthopyroxene and clinopyroxene are commonly intergrown and surrounded by a rim of hornblende (Fig. 7b).

Internal layering in the Marginal Unit is revealed by weak but distinct modal and cryptic layering. Starting at the northern shore, internal layers were sampled across a ~30 m wide section (Fig. 2). Modal variations in the major phases are

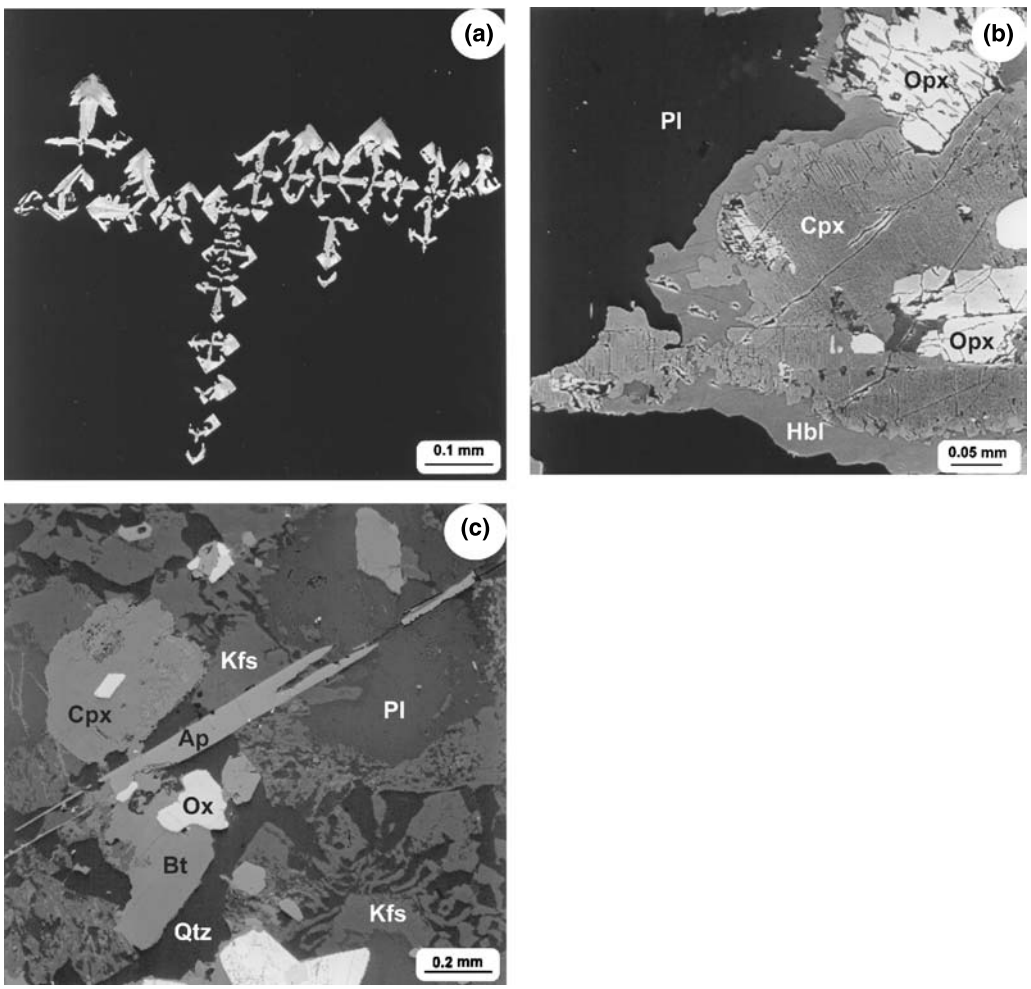

Fig. 7. Back-scattered electron (BSE) images of representative textural features in the Vinga intrusion. (**a**) Arrays of skeletal zircons enclosed in quartz and K-feldspar. Sample 107. (**b**) Intergrown orthopyroxene (Opx) and clinopyroxene (Cpx) with a rim of hornblende (Hbl). Black area represents plagioclase (Pl). Sample 29. (**c**) Tube-shaped apatite (Ap) cut approximately along its c-axis. Other minerals are plagioclase (Pl), K-feldspar (Kfs), quartz (Qtz), biotite (Bt), clinopyroxene (Cpx) and Fe–Ti oxides (Ox). Sample 29

shown in Fig. 8. There is a general decrease in the abundance of plagioclase and orthopyroxene and a slight increase of quartz and hornblende towards the Main Intrusion. Cryptic variations of plagioclase and orthopyroxene range from $An_{50\rightarrow44}$ and $En_{62\rightarrow48}$, respectively (Fig. 9). As in the Main Intrusion, plagioclase is typically mantled by a thin rim of K-feldspar, but is less sericitisised (Table 1). Granophyric intergrowths and skeletal zircons occur here as well as in the Main Intrusion. Apatite from the Marginal Unit generally shows the highest aspect ratios (typically around 20, and locally 100–200), and is commonly hollow (skeletal), forming small tube-like grains (Fig. 7c).

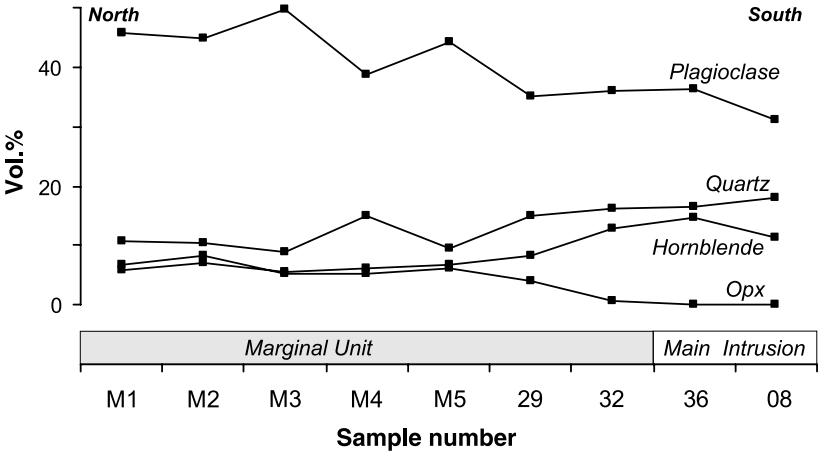

Fig. 8. Modal variation of some major minerals, from north to south, across the Marginal Unit and two samples from the Main Intrusion

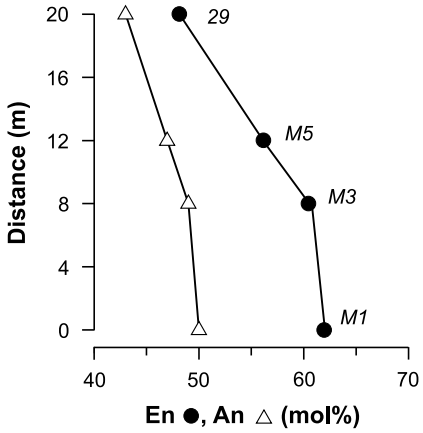

Fig. 9. Cryptic variations of plagioclase and orthopyroxene in samples from the Marginal Unit

Complex plagioclase megacrysts (CPM)

CPM are millimetre- to centimetre-sized (Fig. 3) and occupy ~3–8 vol% of the Main Intrusion and ~1–3 vol% of the Marginal Unit. The megacrysts are subhedral to ovoid, and occur as single crystals or aggregates. They show a cellular/skeletal texture (except the rim, which is non-cellular and normally zoned; Fig. 11), and contain inclusions of mafic minerals (clinopyroxene, orthopyroxene, hornblende and Fe–Ti oxides), K-feldspar and irregular quartz. The term cellular is used here for crystals not perfectly formed, in which the cells contribute to an irregular morphology of the crystal, and includes skeletal forms. The cellular domains have distinct compositions, $An_{34–51}$ and $An_{22–30}$ (Figs. 10, 11; Table 3). In general, the more Ca-rich plagioclase occurs in the core of each cell, rimed by the more Na-rich plagioclase. Each cell is in optical continuity as albite twins are continuous in the core and the rim. Compositions follow approximately those of the matrix plagioclase, i.e. the most calcic CPM are found in the northern Marginal Unit and become more sodic towards and into the Main Intrusion. Normally zoned

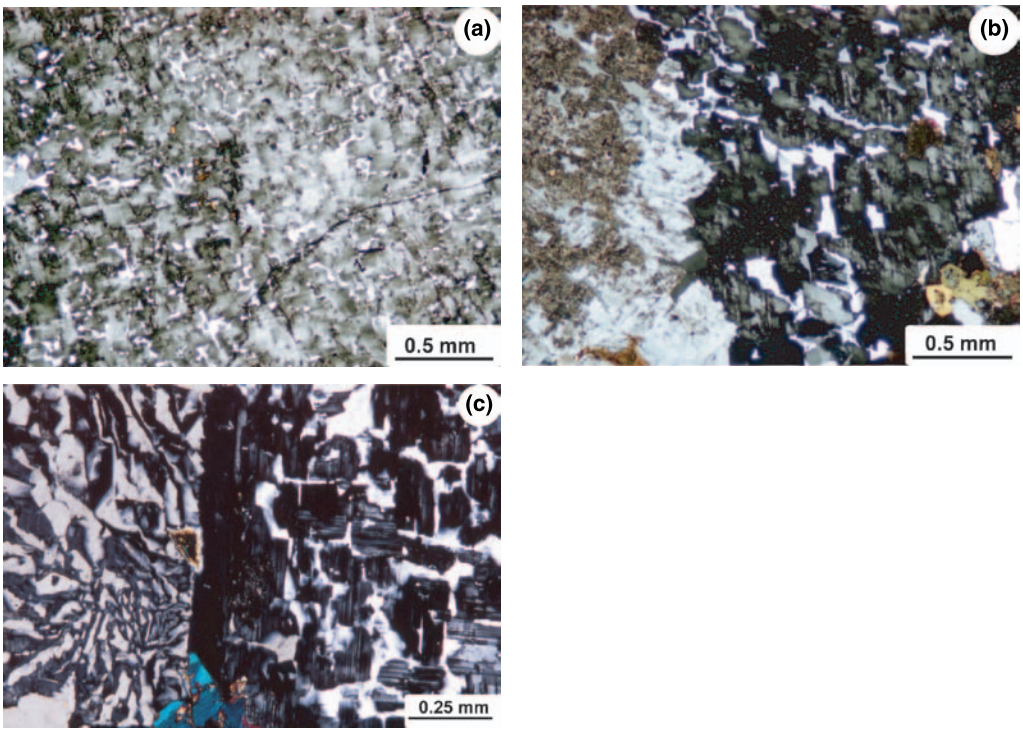

Fig. 10. Photomicrographs of different CPM showing the variation in textural appearance. (**a**) Central part of a ca. 2×3 cm large megacryst showing the cellular morphology of the plagioclase enclosing abundant irregular quartz inclusions (*white*). Plagioclase compositions range from An_{42} (Ca-rich phase; *light grey*) to An_{27} (Na-rich phase; *dark grey*). The Ca-rich plagioclase typically occupies the core of the cells, whereas the peripheral parts are more Na-rich, and usually associated with the quartz. A few clinopyroxene inclusions occur in the centre of the microphotograph. Crossed polarisers. Sample Vi 2. (**b**) Marginal part of a 1.5 cm large megacryst. In this crystal, the cellular morphology includes more distinct 'box-like' cells, still enclosing irregular quartz (*white*), some K-feldspar (dark in this view) and minor hornblende. Plagioclase compositions range from An_{45} to An_{24}. As in (a) the Ca-rich plagioclase typically occurs in the core of the cells. The photomicrograph shows two cellular crystals, each in optical continuity but with different optical extinction; the one to the left shows strong sericitisation. In the lower right part of the photomicrograph the Vinga matrix can be observed. Crossed polarisers. Sample Vi 2. (**c**) Marginal part of a cm-sized megacryst (*right*) in contact with granophyre (*left*). The cellular megacryst, which occurs in a coarse-grained feldspar dominated enclave (see text), is built up of 'box-like' plagioclase cells, enclosing quartz (*white*) and K-feldspar (*black*), with a rim of K-feldspar (*black*). Plagioclase composition ranges from An_{35} (core) to An_{22} (rim) of the cells. Sample 60. Crossed polarisers

rims range from An_{50} to An_{22}, similar to that observed in the matrix plagioclase. The modal content of K-feldspar inclusions increases towards the margin of the megacrysts, and K-feldspar or granophyre commonly occur as an outer rim around the megacrysts (Fig. 11). The mafic minerals are typically in contact with both compositional types of plagioclase (Figs. 10 and 11). The mafic mineral inclusions are generally Fe-enriched compared to those in the matrix. Hornblende is ferro-

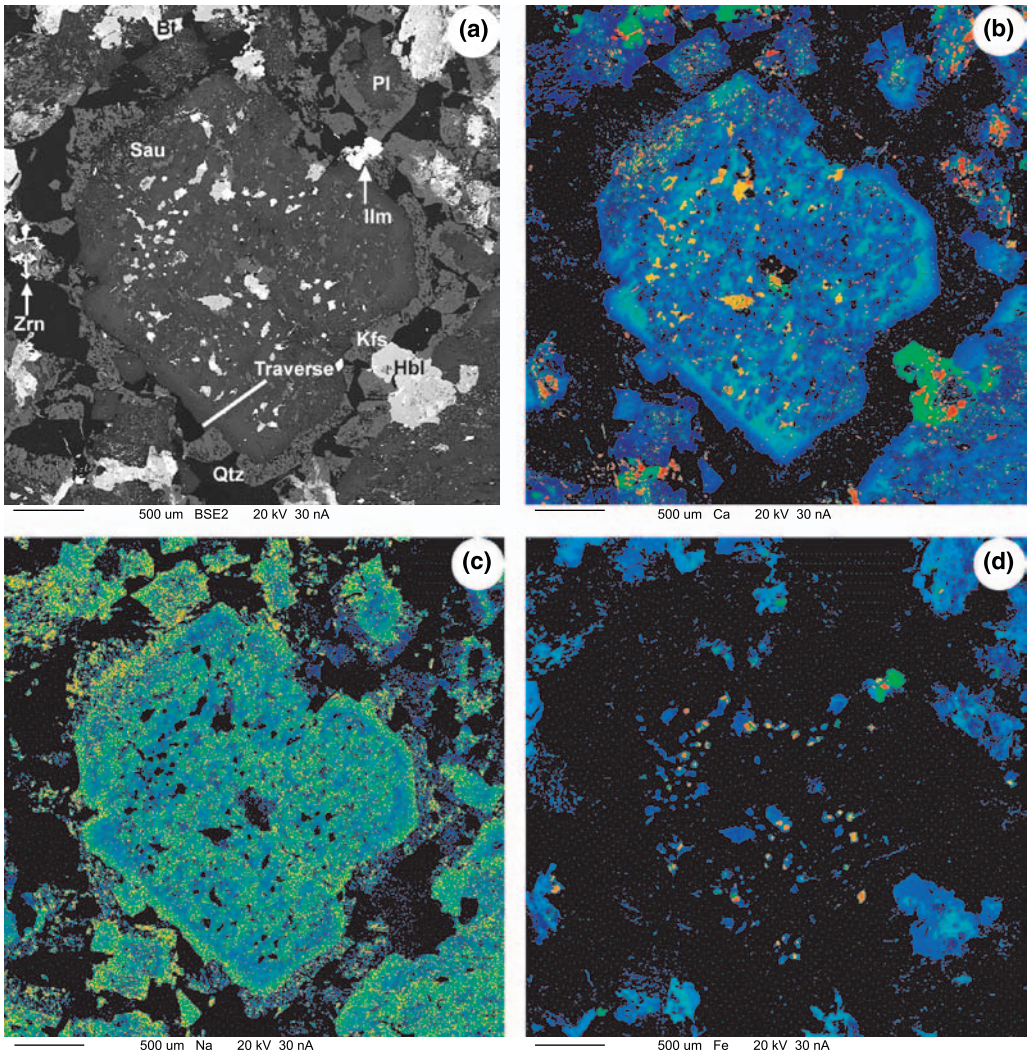

Fig. 11. BSE and element distribution images of a mm-sized CPM, sample 107 (**a**) BSE-image displaying different phases of the CPM and the Vinga matrix. Note the cellular texture of the CPM, the inclusions of mafic silicates (Hbl, Cpx, Opx = *white* to *light grey*), Fe–Ti oxides (Mt, Ilm = *white*), K-feldspar (*grey*) and the homogenous and normally zoned rim (except where it is altered to saussurite (*Sau*)). The CPM as well as matrix plagioclase (*Pl*) is rimmed by K-feldspar or granophyre (*Kfs*). Other minerals in the matrix are hornblende (*Hbl*), quartz (*Qtz*), biotite (*Bt*), ilmenite (*Ilm*) and skeletal zircon (*Zrn*). The white line marks the location of a compositional traverse through the megacryst shown in Fig. 16. (**b**) Ca-distribution image. The different plagioclase phases in the CPM appear as blue (Na-rich) and *greenish blue* (Ca-rich). The Ca-rich plagioclase seems to occur as patches in the Na-rich phase, but is connected to the Ca-rich rim and, the K-feldspar (*black*) is associated to the Na-rich phase. (**c**) Na-distribution image. (**d**) Fe-distribution image. Fe–Mg silicates appear as *blue*, magnetite as red and ilmenite as *green*

hornblende (Mg# 32–33; Fig. 5a), clinopyroxene ranges between augite to ferroaugite ($En_{25-34}Fs_{22-34}Wo_{35-44}$; Fig. 5b) and orthopyroxene is ferro-hypersthene ($En_{37-49}Fs_{46-56}Wo_{3-7}$; Fig. 5b; Table 3).

Table 3. *Representative mineral analyses from the complex plagioclase megacrysts (sample 107) and the mafic microgranular enclaves (sample Vi 11)*

Rock type	Complex plagioclase megacryst										Mafic microgranular enclave			
Sample no.	2:9	2:10	trav:14	trav:20	2:11	2:4	2:3	2:1	2:6	2:5	1:11	1:3	1:2	1:7
Mineral	Pl (Ca)	Pl (Na)	Pl (Ca-rim)	Pl (Na-rim)	Kfs	Opx	Cpx	Hbl	Mt	Ilm	Pl	Opx	Cpx	Ilm
SiO_2 (wt%)	55.05	62.49	56.74	63.16	63.00	48.78	49.50	43.37	0.00	0.00	56.45	50.82	50.72	0.00
TiO_2	0.08	0.04	0.04	0.01	0.00	0.24	0.56	1.58	4.16	50.46	0.04	0.23	0.50	49.34
Al_2O_3	26.31	22.75	25.74	23.18	18.24	0.36	1.02	6.41	1.50	0.00	27.34	0.30	1.19	0.00
FeO	0.28	0.23	0.27	0.15	0.16	33.65	20.66	25.16	87.10	47.81	0.38	30.35	17.51	47.61
MnO	0.00	0.00	0.00	0.01	0.00	0.78	0.44	0.24	0.01	0.86	0.00	0.79	0.49	0.84
MgO	0.00	0.00	0.00	0.00	0.03	12.24	10.59	6.66	0.00	0.00	0.01	13.77	11.43	0.00
CaO	9.83	4.98	8.64	4.53	0.18	2.71	16.63	10.44	0.08	0.04	9.84	3.53	17.84	0.00
Na_2O	5.96	9.00	6.36	9.00	2.38	0.11	0.17	1.84	0.00	0.01	6.10	0.10	0.32	0.00
K_2O	0.21	0.18	0.31	0.43	12.34	0.01	0.00	0.83	0.00	0.01	0.24	0.01	0.00	0.00
Sum	97.72	99.66	98.10	100.45	96.34	98.89	99.56	96.53	92.85	99.20	100.40	99.89	100.01	97.80
Number of oxygens	8					6		23		3	8	6		3
Si	2.540	2.783	2.595	2.787	2.986	1.969	1.941	6.874		0.000	2.534	1.993	1.953	0.000
Ti	0.003	0.001	0.001	0.000	0.000	0.007	0.016	0.189		0.976	0.001	0.007	0.015	0.970
Al	1.430	1.194	1.388	1.206	1.019	0.017	0.047	1.197		0.000	1.446	0.014	0.054	0.000
Fe	0.011	0.008	0.010	0.005	0.006	1.136	0.677	3.335		1.028	0.014	0.996	0.564	1.041
Mn	0.000	0.000	0.000	0.000	0.000	0.027	0.015	0.032		0.019	0.000	0.026	0.016	0.019
Mg	0.000	0.000	0.000	0.000	0.002	0.737	0.619	1.574		0.000	0.001	0.805	0.656	0.000
Ca	0.486	0.238	0.424	0.214	0.009	0.117	0.698	1.773		0.001	0.473	0.148	0.736	0.000
Na	0.533	0.777	0.564	0.770	0.219	0.009	0.013	0.565		0.001	0.531	0.008	0.024	0.000
K	0.013	0.010	0.018	0.024	0.746	0.001	0.000	0.168		0.000	0.014	0.000	0.000	0.000
Σ cations	5.015	5.012	5.000	5.007	4.987	4.020	4.026	15.706		2.025	5.014	3.997	4.017	2.030
An/En	47.09	23.19	42.11	21.23	0.95	36.54	30.81				46.48	40.77	33.27	
Ab/Fs	51.68	75.81	56.09	76.38	22.45	56.32	33.70				52.15	50.40	28.60	
Or/Wo	1.22	1.00	1.80	2.39	76.60	5.81	34.76				1.37	7.51	37.32	
Mg#						39.35	47.76	32.07				44.72	53.78	
Xgk										0.00				0.00
Xpy										0.02				0.02
Xilm										0.98				0.98
Hornblende classification name								ferro-hornblende						

Mol.% An = 100Ca/(Ca + Na + K); Ab = 100Na/(Ca + Na + K); Or = 100K/(Ca + Na + K)
Mol.% En = 100Mg/(Mg + Fe + Mn + Ca); Fs = 100Fe/(Mg + Fe + Mn + Ca); Wo = 100Ca/(Mg + Fe + Mn + Ca); Mg# = 100Mg/(Mg + Fe)
Xgk = Mg; Xpy = Mn; Xilm = 1 − (Xgk + Xpy)
The spreadsheet program PROBE-AMPH (Tindle and Webb, 1994) was used to determine classification names for hornblende

Aplitic dykes and granitic segregations

The Vinga intrusion is cut by a few NNE-trending aplitic dykes (Fig. 2). They range in thickness from a few cm to 0.5 m, and enclose drusy cavities towards their centres. Even though these dykes have sharp external contacts, they commonly have convolute or en echelon forms which indicate that they intruded the Vinga intrusion when it was still semi-plastic.

Decimetre-sized granitic segregations are sparsely distributed in the Main Intrusion, most commonly in the ESE part and close to the aplitic dykes. They are medium-grained and rich in K-feldspar (Table 1 and Fig. 4). The granitic segregations contain millimetre- to centimetre-sized miarolitic cavities infilled with central quartz + chlorite and peripheral K-feldspar. Miarolitic cavities are also found in the Main Intrusion, but they are not as abundant as in the granitic segregations. The granitic segregations contain biotite and hornblende, whereas the predominant mafic phase in the aplitic dykes is chlorite. The hornblende is Fe-enriched relative to the rest of the intrusion and ranges from ferri-tschermakitic to magnesio-hastingsitic hornblende (Mg# = 31–35; Table 2 and Fig. 5a). Accessory phases in both the dykes and the segregations include apatite and skeletal zircon.

Mafic microgranular enclaves (MME)

Rounded, mafic enclaves of millimetre- to centimetre-size are scattered through the intrusion (Fig. 3b). They are fine-grained, equigranular, and constitute <1 vol% of the intrusion. In order of decreasing abundance, the enclaves consist of plagioclase (An_{43-51}), clinopyroxene ($En_{33-36}Fs_{26-29}Wo_{35-40}$), Fe–Ti oxides, orthopyroxene ($En_{40-44}Fs_{49-53}Wo_{3-10}$), biotite, hornblende (ferrian-magnesio hornblende; Mg# = 42–50), apatite ± quartz ± K-feldspar (Table 1). Some of the orthopyroxene contain > Wo_5, i.e. pigeonite composition. Both the clinopyroxene and orthopyroxene are enriched in Fe relative to the host rock (Fig. 5b; Table 3). In places, the MME also contain a few megacrysts of plagioclase and hornblende. Apatites are typically acicular.

Coarse-grained feldspar-dominated enclaves

The Vinga intrusion locally contains irregular, decimetre- to metre-sized enclaves of coarse-grained plagioclase and fine-grained granophyre with aggregates of interstitial hornblende, chlorite, epidote, calcite ± pyrite (Fig. 3c). Cavities lined with quartz + calcite + chlorite ± hornblende ± epidote are common, mainly in the granophyric matrix. The granophyre also contains accessory amounts of acicular apatite and ilmenite (aspect ratios of 12–26). The subhedral plagioclase consists of cellular/(skeletal) plagioclase, commonly sericitised, containing abundant inclusions of mafic minerals, K-feldspar and quartz, i.e. CPM. The MME are typically spatially associated with these coarse-grained enclaves.

Xenoliths

The most prominent type is quartz fragments mantled by hornblende (Fig. 3b). Gneissic xenoliths also occur, but are much more sparsely distributed. A third, rare

type, includes 'pegmatitic' coarse-grained feldspar ± quartz. The numerous millimetre- to metre-sized quartz fragments are remarkably evenly distributed throughout the intrusion. They show different shapes, from rounded to angular, but most of them are brick-shaped, resembling randomly oriented pieces of vein quartz. The quartz is medium- to coarse-grained, usually very pure in terms of inclusions and displays undulatory extinction. All the quartz fragments feature a millimetre-wide rim consisting of hornblende, or an inner and an outer hornblende rim with granophyre between. The hornblende rims consist of euhedral to subhedral, ferri-magnesio-hornblende (Mg# = 50–54). The granophyre is irregularly distributed around the xenoliths. Acicular apatite is common in the granophyre.

In addition to the quartz fragments, there are some decimetre- to metre-sized quartzitic fragments. These fragments consist of alternating layers of fine-grained, granoblastic quartz with minor feldspar. Like the quartz fragments, they exhibit hornblende ± granophyre rims toward the matrix.

Decimetre- to metre-sized gneissic enclaves are not as common as the quartz fragments and are concentrated in the western part of Vinga Island. These enclaves are primarily migmatised paragneisses, rocks similar to the enclosing SLM, although a few orthogneisses and amphibolites were observed. Most of the gneiss enclaves have strongly resorbed margins (Fig. 3a), indicating that the Vinga magma experienced some crustal contamination.

Whole-rock geochemistry

Major and trace element analyses for the Vinga intrusion are reported in Table 4. With the exception of the granitic segregation and aplitic dyke, all samples are ferroan, with high contents of Ti, P, K, and high field strength elements (HFSE). The SiO_2 content of the granitic segregation and the aplitic dyke exceeds 70 wt%, ranges from 59.3 to 62.4 wt% in the Main Intrusion, from 55.4 to 59.2 wt% in the Marginal Unit, and from 47.2 to 56.3 wt% in the MME. In the classification of Frost et al. (2001), the intrusion is ferroan with an alkali-calcic affinity (Fig. 12). The rocks are metaluminous and form a roughly linear trend of increasing A/CNK (0.74–0.98) with increasing SiO_2. Fluorine was analysed in one sample from each of the major rock units, including the Marginal Unit, the Main Intrusion and the granitic segregation. All three samples have high F contents, ranging up to 0.9 wt%. The high contents of F, Fe and HFSE shown by the intrusion are typical for A-type or AMCG-type granitoids (e.g. Whalen et al., 1987; Sallet, 2000; Frost et al., 2002). The ferric iron content was analysed in the same three samples. The ferric/ferrous ratio, which is dependent on the oxidizing state, shows increasing values with increasing SiO_2.

In Harker diagrams of major and trace elements the evolution of the Vinga rocks define trends that can be divided into three segments, separated by kinks in the diagrams (Fig. 13). The first segment represents the evolution from the Marginal Unit to the more mafic end of the Main Intrusion, the second the evolution within the Main Intrusion, and the third the evolution towards the granitic segregation. The Marginal Unit is characterised by higher contents of MgO, Fe_2O_3, TiO_2, CaO, Al_2O_3, Ni, and Sr than the Main Intrusion, but lower K_2O, Rb, Ba, Eu, Th, Ce, Y, Nb, and Fe#, and approximately equal amounts of Na_2O, P_2O_5, and Zr.

Table 4. *Whole-rock geochemistry of samples from the Vinga intrusion*

Rock type	Main Intrusion								Marginal Unit							MME			Granitic seg. dyke	
Colour	Grey					Reddish grey														
Sample no.	8	36	60	64	107	74	90	94	M1	M2	M3	M4	M5	29	32	Vi11	F1	F2	24	5
SiO_2 (wt.%)	59.30	60.09	59.78	60.44	61.87	61.67	62.42	62.23	55.45	55.47	55.51	56.10	56.23	56.45	59.23	47.19	53.38	56.25	70.73	70.79
TiO_2	1.81	1.73	1.80	1.71	1.56	1.60	1.48	1.49	2.74	2.74	2.69	2.57	2.61	2.53	2.03	3.64	2.67	2.26	0.59	0.58
Al_2O_3	14.15	14.05	13.96	14.02	14.03	13.90	13.81	13.94	14.65	14.66	14.71	14.73	14.56	14.47	14.24	13.16	14.44	13.91	13.44	12.84
$Fe_2O_{3(tot)}$	9.78	9.42	9.65	9.23	3.22	8.67	8.28	8.24	11.20	2.66	11.18	10.81	11.06	10.94	9.62	18.25	11.86	11.24	2.17	3.83
FeO	–	–	–	–	4.80	–	–	–	–	7.70	–	–	–	–	–	–	–	–	1.30	–
MnO	0.12	0.11	0.12	0.11	0.10	0.10	0.09	0.09	0.14	0.14	0.13	0.12	0.15	0.12	0.11	0.23	0.16	0.14	0.02	0.04
MgO	2.2	2.10	2.09	2.08	1.75	1.90	1.72	1.74	3.45	3.43	3.41	3.16	3.28	3.17	2.47	4.30	2.94	2.35	0.32	0.74
CaO	4.56	4.27	4.49	4.24	3.94	3.81	3.42	3.55	5.19	5.21	5.25	5.21	5.00	5.00	4.51	6.03	5.97	5.48	0.93	1.56
Na_2O	3.36	3.33	3.33	3.38	3.45	3.33	3.41	3.45	3.45	3.44	3.47	3.45	3.43	3.40	3.44	2.77	3.42	3.26	2.95	3.92
K_2O	3.27	3.32	3.32	3.42	3.71	3.69	3.89	3.73	2.67	2.69	2.66	2.78	3.43	2.82	3.24	2.21	3.10	3.31	6.59	3.89
P_2O_5	0.57	0.52	0.55	0.50	0.46	0.46	0.43	0.44	0.58	0.58	0.57	0.58	0.53	0.53	0.51	0.47	0.82	0.89	0.06	0.29
LOI	0.85	1.06	0.90	0.84	0.57	0.87	1.04	1.11	0.43	0.38	0.37	0.43	0.31	0.56	0.59	1.96	0.62	0.31	0.77	1.44
Total	99.97	100.00	99.99	99.97	100.00	100.00	99.99	100.01	99.95	99.96	99.95	99.94	99.95	99.99	99.99	100.12	99.38	99.41	100.01	99.92
F	–	–	–	–	0.9	–	–	–	–	0.8	–	–	–	–	–	–	–	–	0.5	–
Fe#	69.2	69.4	70.0	69.2	71.2	69.7	70.8	70.5	62.1	62.3	62.3	63.3	63.0	63.5	66.3	68.2	67.1	70.7	85.1	72.3
A/CNK	0.82	0.83	0.81	0.83	0.83	0.85	0.86	0.86	0.81	0.81	0.81	0.81	0.82	0.82	0.82	0.74	0.73	0.74	0.98	0.95
As (ppm)	1.45	1.49	1.39	1.35	1.40	1.48	0.83	1.26	0.92	0.90	0.81	0.94	1.05	0.91	1.08	1.62	b.d.	b.d.	0.37	5.94
Be	1.94	2.52	2.54	2.72	3.02	2.04	2.54	2.27	2.25	2.50	2.59	2.29	3.76	1.76	1.90	3.32	2.22	3.22	2.99	1.60
Bi	0.07	0.07	0.06	0.09	0.06	0.09	0.06	b.d.	0.05	0.06	0.07	0.08	0.07	b.d.	0.07	0.19	0.13	b.d.	0.23	<0.05
Cr	79	89	77	73	86	77	122	113	157	139	143	109	105	101	109	191	125	159	144	136

(*continued*)

Table 4 (*continued*)

Rock type	Main Intrusion								Marginal Unit							MME			Granitic seg. dyke	
Colour	Grey					Reddish grey														
Sample no.	8	36	60	64	107	74	90	94	M1	M2	M3	M4	M5	29	32	Vi11	F1	F2	24	5
Cd	0.31	0.27	0.26	0.22	0.30	0.19	0.32	0.33	0.30	0.30	b.d.	b.d.	b.d.	b.d.	0.16	b.d.	0.40	0.40	0.31	<0.15
Co	20.2	18.4	19.3	18.6	14.3	14.9	13.2	13.3	31.6	30.4	29.6	27.2	31.8	29.4	23.0	58.2	26.1	22.2	3.3	7.3
Cs	4.07	3.04	2.59	3.44	1.74	1.38	1.02	1.07	1.28	1.39	1.46	1.57	1.64	2.59	2.19	7.45	4.83	4.18	0.99	0.76
Cu	19.0	16.4	16.2	16.2	13.6	15.1	12.9	13.4	21.4	22.1	21.8	18.5	24.9	22.4	18.7	86.6	19.1	15.7	7.70	8.8
Zn	153	155	158	156	134	132	125	129	158	162	156	149	172	152	147	271	178	177	59	39
Pb	21.39	24.98	24.45	22.44	17.10	18.27	18.8	18.72	13.3	14.3	14.3	14.2	14.5	17.48	17.78	11.2	13.9	21.0	28.81	8.14
Ni	18.1	18.0	17.4	17.1	13.7	14.2	13.6	12.7	45.3	45.5	43.5	36.5	47.8	40.6	27.7	51.2	26.0	23.6	3.6	8.7
Sb	b.d.	0.10	b.d.	b.d.	b.d.	b.d.	b.d.	b.d.	b.d.	b.d.	b.d.	b.d.	b.d.	b.d.	0.10	0.58	b.d.	b.d.	b.d.	b.d.
Sn	3.03	2.87	2.92	3.08	2.85	2.94	3.26	3.29	2.77	2.73	2.70	2.79	2.69	2.59	2.77	2.81	2.49	2.94	4.96	1.44
Sc	14.9	14.4	14.9	14.3	13.3	13.4	12.8	12.7	–	–	–	–	–	15.6	14.4	–	–	–	5.2	8.1
Mo	2.48	2.39	2.46	2.20	2.30	2.65	2.14	2.50	2.00	2.02	2.22	1.93	2.09	2.24	2.19	1.94	2.29	2.94	1.49	0.31
V	92.0	86.0	90.7	86.9	71.6	73.6	64.9	65.6	152	145	142	137	157	133.6	104.5	412	143	107	8.7	30.2
W	0.85	0.84	0.89	0.82	0.84	0.95	0.88	1.00	0.60	0.62	0.60	0.61	0.73	0.67	0.83	1.19	0.59	0.75	1.50	0.57
Ga	28.3	26.8	27.0	27.2	26.7	27.1	26.5	26.8	26.0	27.1	26.1	25.6	27.5	26.3	25.8	30.0	26.9	27.8	26.1	16.8
Ge	1.23	1.28	1.27	1.24	1.09	1.17	1.03	1.07	1.71	1.59	1.60	1.71	1.83	1.23	1.28	2.60	1.63	1.81	1.20	0.59
In	b.d.	0.12	0.12	0.12	b.d.	0.11	b.d.	0.13	0.11	0.12	0.12	0.11	0.12	b.d.	0.11	0.23	0.17	0.16	b.d.	b.d.
Ba	865	945	854	866	846	847	888	965	757	773	748	758	865	846	851	675	683	780	1269	1026
Rb	113	109	114	109	118	113	125	114	81.5	79.4	75.9	78.2	95.9	91	106	133	125	118	164	121
Sr	376	354	352	344	301	295	274	295	444	446	435	421	414	420	390	413	402	364	103	134
Ta	1.72	1.68	1.68	1.73	1.58	1.59	1.64	1.63	1.32	1.36	1.51	1.36	1.54	1.51	1.56	1.61	1.53	1.63	1.21	1.47
Nb	23.1	22.3	23.0	22.6	21.9	21.9	22.1	22.2	19.1	19.2	20.2	18.6	20.8	19.9	21.1	21.5	21.7	22.6	12.2	14.4
Hf	11.27	11.29	10.95	10.97	11.03	11.40	12.1	11.78	9.24	9.42	9.57	9.65	10.0	10.68	10.67	8.20	8.19	9.15	17.51	4.91

(*continued*)

Table 4 (*continued*)

Rock type	Main Intrusion								Marginal Unit							MME			Granitic seg. dyke	
Colour	Grey					Reddish grey														
Sample no.	8	36	60	64	107	74	90	94	M1	M2	M3	M4	M5	29	32	Vi11	F1	F2	24	5
Zr	423	434	422	427	447	452	472	464	426	459	431	451	454	414	432	330	320	367	637	191
Y	69.0	67.7	68.4	67.4	65.4	65.8	65.7	64.8	48.8	49.8	50.3	50.6	51.3	53.1	61.2	59.3	58.4	69.7	49.1	37.8
Th	12.66	12.96	12.47	13.13	12.96	12.90	13.17	13.50	7.70	8.69	8.52	8.99	8.84	11.24	12.42	2.85	5.48	7.55	21.15	8.80
U	3.21	3.30	3.07	3.42	3.02	3.31	3.19	3.35	2.38	2.53	2.55	2.92	2.68	2.50	3.08	0.97	1.82	2.35	4.86	3.81
La	65.2	61.4	63.0	64.0	61.8	61.1	61.8	62.4	50.3	51.8	48.8	51.4	56.4	55.3	59.9	35.8	51.9	62.3	59.4	30.5
Ce	144.5	137.6	139.1	141.5	136.4	134.9	136.8	137.0	113	115	111	113	124	120.9	130.4	79.9	117	140	122.1	65.6
Pr	18.9	17.6	18.0	18.0	17.6	17.2	17.4	17.6	14.1	14.4	14.3	14.6	14.6	15.6	16.8	10.7	15.4	18.5	15.1	8.4
Nd	80.9	75.2	76.5	75.9	72.9	73.5	73.7	72.7	58.4	59.9	59.0	60.7	61.6	66.2	70.1	45.1	64.6	78.1	56.1	32.9
Sm	17.3	16.3	16.6	16.7	16.0	16.5	15.6	16.4	11.8	12.1	12.5	12.3	13.1	13.6	15.1	11.0	14.1	16.9	11.1	7.2
Eu	4.16	3.93	3.70	3.69	3.58	3.46	3.37	3.54	3.12	3.22	3.31	3.14	3.27	3.53	3.48	4.31	4.02	4.04	2.58	1.47
Gd	14.4	14.0	13.7	14.4	13.4	13.4	13.0	13.4	11.0	11.5	10.7	11.7	10.9	11.9	12.6	10.5	12.7	15.3	9.4	6.7
Tb	2.19	2.19	2.16	2.17	2.04	2.00	1.98	2.03	1.56	1.65	1.61	1.69	1.64	1.77	1.89	1.74	1.92	2.31	1.51	1.02
Dy	12.3	12.4	12.8	12.9	11.8	11.5	11.2	11.3	8.7	9.0	8.8	9.3	9.3	9.9	10.8	10.4	11.1	13.2	9.0	6.1
Ho	2.52	2.40	2.39	2.42	2.28	2.16	2.18	2.25	1.62	1.75	1.69	1.81	1.83	2.06	2.16	2.10	2.07	2.46	1.86	1.28
Er	6.68	6.04	6.40	6.16	5.76	5.81	5.95	5.79	4.09	4.39	4.38	4.60	4.80	5.04	5.44	6.02	5.65	6.59	4.77	3.59
Tm	0.958	0.944	0.935	1.01	0.875	0.970	0.928	0.894	0.674	0.679	0.664	0.719	0.721	0.746	0.851	0.898	0.796	0.928	0.730	0.582
Yb	6.22	6.17	6.32	6.78	5.91	6.34	6.17	6.00	4.17	4.25	4.28	4.31	4.71	4.80	5.55	6.02	5.10	5.93	4.83	3.88
Lu	0.957	0.867	0.885	0.888	0.888	0.825	0.835	0.815	0.610	0.639	0.669	0.701	0.725	0.686	0.764	0.964	0.779	0.892	0.696	0.523

b.d. Below detection limit. $Fe\# = 100 * Fe_2O_{3,tot}/(Fe_2O_{3,tot} + MgO)$

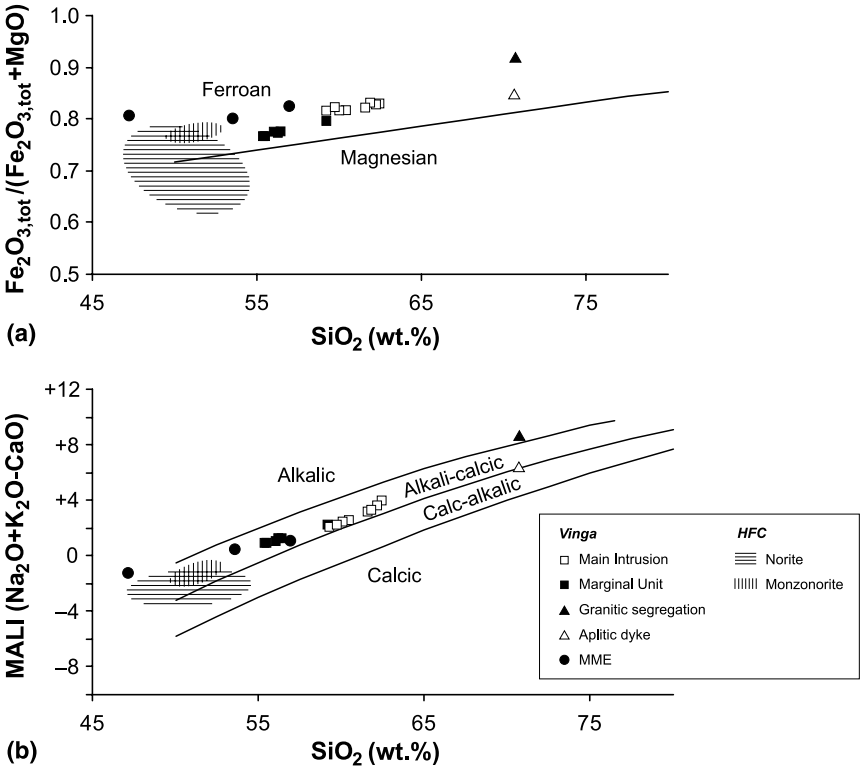

Fig. 12. Geochemical classification of granitoid rocks according to Frost et al. (2001). For comparison, rocks from the Hakefjorden Complex are included. (**a**) Plot of SiO_2 vs Fe# ($Fe_2O_{3tot}/(Fe_2O_{3tot} + MgO)$ showing the ferroan nature of the Vinga intrusion. (**b**) Plot of SiO_2 vs. MALI (modified alkali lime index; $Na_2O + K_2O$–CaO) displaying the alkali-calcic affinity of the intrusion

The compositional variation within the Main Intrusion and further to the granitic segregation is characterized by decreasing MgO, Fe_2O_3, TiO_2, CaO, Al_2O_3, P_2O_5, Ni, Sr, Eu, Sr, Ce, Y, and Nb, but increasing K_2O, Rb, Ba, Zr, Th, and Fe#.

The chemistry of the Vinga intrusion is compared with that of the mafic, penecontemporaneous, late Sveconorwegian Hakefjorden Complex (HFC) rocks and the Göteborg dykes (Fig. 13). The HFC rocks are separated into norites and the generally more evolved monzonorites (Årebäck, 2001). The Göteborg dykes are distinct from the HFC because of their high Al_2O_3, Na_2O, Sr, and low Zr contents.

MMEs define trends separate from those between the Main Intrusion and Marginal Unit, having elevated contents of LILE, and a few HFSE (Fig. 13). The most basic Vinga-MME resembles the HFC-norite with some exceptions, e.g. Fe, Rb, and Eu, which are higher in the Vinga enclave. The MMEs appear to form an indistinct trend plotting roughly between the more evolved part of the HFC-norites and the Vinga Main Intrusion.

The composition of the aplitic dyke is notably different from the granitic segregation in terms of Na_2O, K_2O, P_2O_5, Zr, Rb and Ba (Fig. 13 and Table 4), and the dyke shows geochemical similarity with the metasediments of SLM.

The Σ REE contents are 350–377 ppm in the Main Intrusion and 282–336 ppm in the Marginal Unit, 225–367 ppm in the MME, and 170 ppm in the aplitic dyke. Chondrite-normalised REE patterns (Fig. 14) for the Main Intrusion, the Marginal Unit and the granitic segregation are subparallel, with moderate enrichment of LREE relative to HREE [$(La/Yb)_n = 6.4–8.3$], suggesting that no HREE-retaining

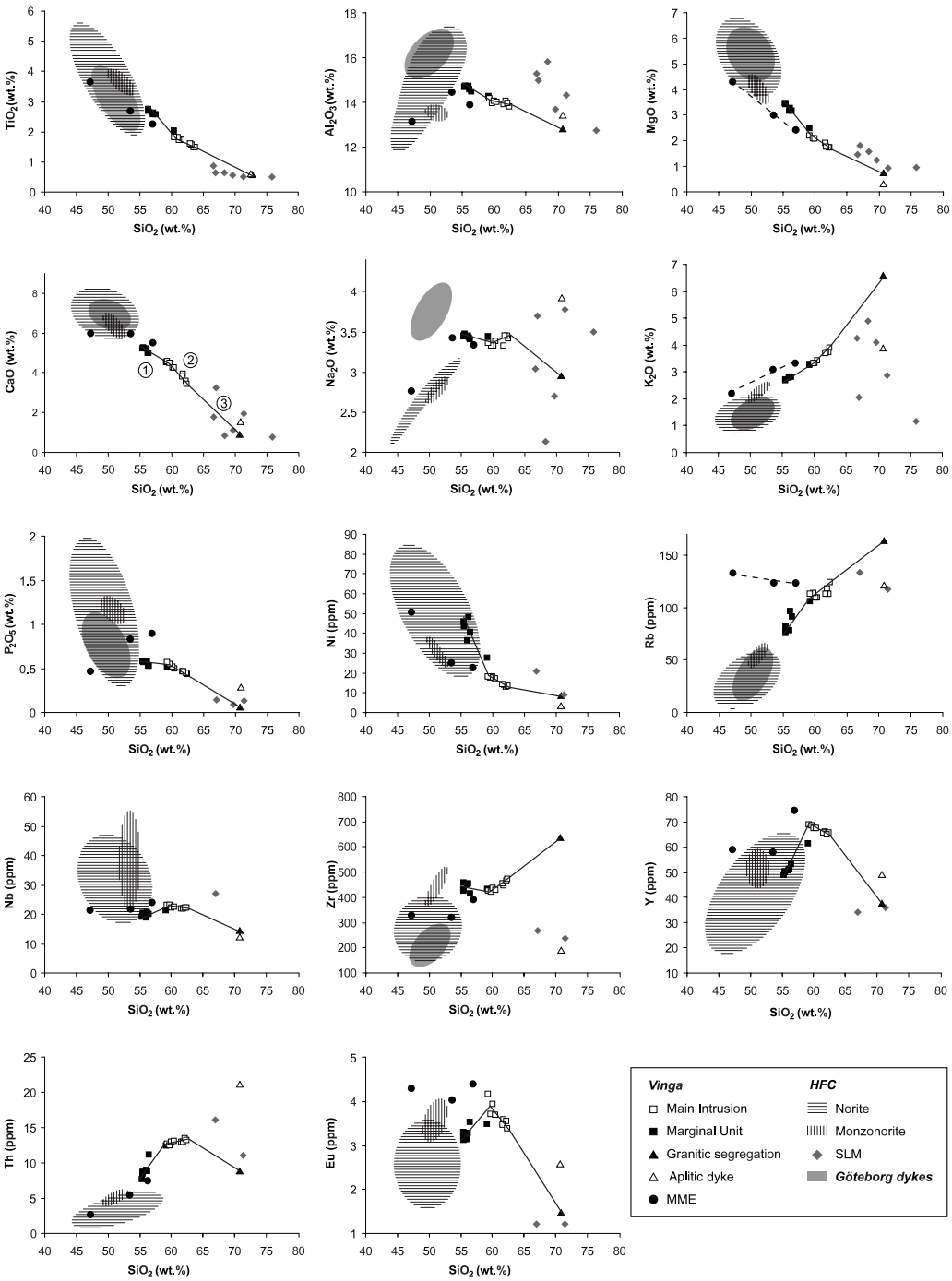

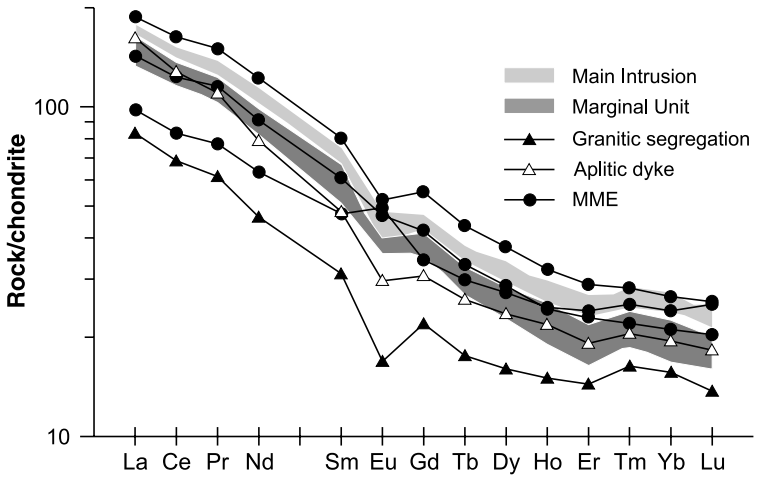

Fig. 14. REE patterns of the Vinga intrusion samples. Data are normalised to chondrite values of Taylor and McLennan (1985)

phase (e.g. garnet) was present in the source after melting. All rocks of the intrusion (except some MMEs) display negative Eu anomalies ($Eu/Eu^* = 0.71$–0.87). The MMEs on the other hand, show both slightly positive and negative Eu anomalies ($Eu/Eu^* = 1.23$–0.77), compatible with a wide range in modal plagioclase contents (Fig. 14). The granitic segregation differs from the other samples by its slightly lower content of intermediate REE.

U–Pb geochronology

More than hundred zircon crystals with skeletal morphology were recovered from sample 107. This sample represents the same rock type as was collected by Åhäll and Schöberg (1999), which yielded a highly discordant U–Pb zircon age of 963 ± 17 Ma (2σ; MSWD $= 1.3$) by conventional TIMS analysis. These authors

Fig. 13. Harker variation diagrams for selected major and trace elements of the Vinga intrusion. Compositional fields for the Hakefjorden complex (HFC) and the Göteborg dykes have been included for comparison (Årebäck, 1995; Hellström et al., 2004; Johansson, 1997). The compositional evolution of the Vinga rocks can be separated into three segments, as indicated in the CaO diagram: (1) From the Marginal Unit to the Main Intrusion, characterised by the separation of ortho- and clinopyroxene, Fe–Ti oxides and plagioclase, (2) in the Main Intrusion the melt becomes saturated in apatite, which is removed together with plagioclase, clinopyroxene, oxides and amphibole, and (3) represents the removal of residual melt of the granitic segregations from a crystal mush of the phases in (2). The fractionating assemblage does not contain zircon, biotite, or K-feldspar. Extensions of the trends do not result in a defined mafic end member. The MMEs represent variable mixtures of a mafic end member similar to the HFC norites and the Vinga Main Intrusion. Rb and K_2O diagrams show that they have been subjected to selective fluid enrichment of LILE from the host rock. The aplitic dyke has geochemical similarities with the SLM metasediments

described zircons from their concentrate as '... euhedral and elongate with aspect ratios of ~4′ with some grains having ' ... irregular surfaces or even corroded appearance'. Surprisingly, only one such prismatic crystal was found among the

Table 5. *Ion microprobe U–Th–Pb data for skeletal zircons of Vinga sample 107 (Swedish national grid 639800/124840; latitude 57′38.1952″/longitude 11′35.4825″)*

Crystal	[U] ppm	[Pb] ppm	Th/U	f_{206}[a] %	Isotopic ratios				Ages (Ma)[b]		Disc[c] %
					$^{206}Pb/^{238}U$	$\pm\sigma$	$^{207}Pb/^{206}Pb$	$\pm\sigma$%	$^{206}Pb/^{238}U$	$^{207}Pb/^{206}Pb$	
5	848	174	0.69	0.04	0.1598	2.05	0.07078	0.3	956 ± 18	951 ± 7	
6	321	64	0.77	0.14	0.1533	2.06	0.06774	0.8	919 ± 18	861 ± 15	0.2
15	201	39	0.52	0.06	0.1563	2.06	0.07036	0.7	936 ± 18	939 ± 13	
31a	1310	278	0.76	<0.01	0.1634	2.06	0.06918	0.7	976 ± 19	904 ± 15	1.6
31b	3413	530	1.30	0.50	0.1062	2.14	0.06410	0.8	650 ± 13	745 ± 16	−6.2
63a	1023	224	0.85	0.01	0.1649	2.05	0.07000	0.4	984 ± 19	928 ± 7	1.4
63b	1328	294	0.93	0.01	0.1637	2.05	0.07037	0.4	977 ± 19	939 ± 8	
63c	1959	441	1.01	0.01	0.1634	2.10	0.07079	0.2	976 ± 19	951 ± 5	
80a	820	170	0.69	<0.01	0.1617	2.05	0.07106	0.3	966 ± 18	959 ± 7	
80b	1484	241	0.96	0.32	0.1192	2.07	0.06651	0.5	726 ± 14	822 ± 9	−7.5
89	437	85	0.53	1.10	0.1587	2.06	0.06919	0.9	949 ± 18	904 ± 17	
108	1148	232	0.46	0.01	0.1672	2.06	0.07055	0.3	997 ± 19	944 ± 6	1.1

[a] Percentage of ^{206}Pb contributed by common ^{206}Pb, estimated from measured ^{204}Pb assuming Stacy and Kramers (1975) model

[b] Errors on ages are 1σ

[c] Degree of discordance; positive numbers are reverse discordant. Blanks indicate concordance within 2σ

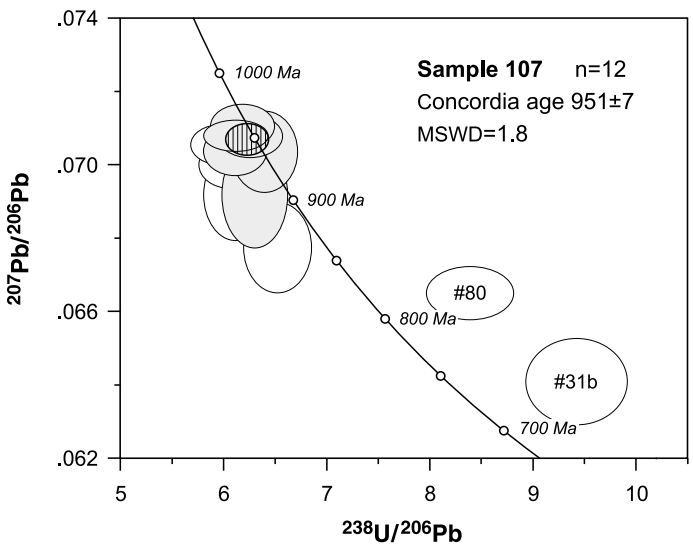

Fig. 15. Tera-Wasserburg diagram showing analytical data for skeletal zircons from sample 107. Shaded error ellipses indicate concordant analyses; the striped error ellipse is their weighted mean or concordia age. Error ellipses are 1σ; concordia tick marks are every 50 Ma

skeletal zircons of sample 107. Back-scattered electron and cathodoluminescence images of the skeletal zircons reveal that they are rather structureless, apart from occasional, vague angular growth zoning (Fig. 7a), or irregular, back-scattered electron-dark embayments. The single prismatic crystal preserves a distinct oscillatory zoning, typical of magmatic crystallization.

Judging from textural relationships, skeletal zircons are associated with interstitial phases such as quartz and K-feldspar, and therefore must have crystallised from the magma. These zircons should constrain the emplacement age for the Vinga intrusion. Twelve ion microprobe (SIMS) U–Th–Pb analyses were performed on 8 skeletal fragments (Table 5). Except for some indication of Pb loss in analyses 31b and 80, these data are mostly near-concordant within error (Fig. 15). For the six concordant analyses, a $^{207}Pb/^{206}Pb$-$^{238}U/^{206}Pb$ *concordia age* (Ludwig, 1998) of 951 ± 7 Ma (2σ; MSWD = 1.8) was obtained, which is considered the best estimate of the crystallization age of this sample.

Estimates of crystallisation conditions

Pressures and temperatures were estimated for the different units where appropriate mineral assemblages occur are summarised in Table 6. The pressure of emplacement crystallisation is estimated to be $\leq$2 kbar using the temperature-corrected Al-in-hornblende barometer of Anderson and Smith (1995). For temperature estimates, the two-pyroxene QUILF thermometer (Ca partitioning; Anderson et al., 1993), the amphibole-plagioclase thermometer of Holland and Blundy (1994) and the zircon and apatite saturation thermometers of Watson and Harrison (1983) and Harrison and Watson (1984) were used. For the amphibole-plagioclase thermometer, the calibration reaction edenite + 4 quartz = tremolite + anorthithe was used. A pressure of 2 kbar was assumed for the amphibole-plagioclase thermometer and 5 kbar for the two-pyroxene thermometer. P–T was also estimated using clinopyroxene-liquid thermobarometers calibrated for basic to silicic compositions by Putrika et al. (2003).

Two-pyroxene temperatures of 1015 ± 20 °C were determined for the Marginal Unit, whereas the pyroxenes in the MME and the CPM yielded lower temperatures of equilibration, 880 ± 10 °C and 870 ± 50 °C, respectively. The clinopyroxene geobarometer of Nimis (1999), based on structural and chemical response to pressure variations, was applied to core and rim compositions from the Marginal Unit (T = 1015 and 950 °C, respectively). The compositions of the Vinga rocks are close to those used to calibrate the barometer for 'mildly alkaline' (MA) systems, and yield results consistently in the range 4.0–6.0 kbar. Similarly, the clinopyroxene thermobarometer calibrated for compositions up to $SiO_2 = 71\%$ by Putirka et al. (2003) yielded maximum pressures in the range 4.6–6.6 kbar for rocks in the Marginal Unit and the MME, and temperatures of 1090–1100 °C. These data indicate subemplacement pressures for early pyroxene crystallization, at mid-crustal depths of 15–20 km. Additionally, certain clinopyroxenes, e.g. in the CPM, indicate crystallization during emplacement at pressures as low as 2.0–0.7 kbar and 1050 °C. The composition of the clinopyroxenes and whole rocks yielding these results generally satisfies the test according to the clinopyroxene saturation model of Putirka (1999).

Table 6. *Summary of P–T estimates*

Unit	Pressure (kbar)			Temperature (°C)				
	Al-in Hbl (Anderson and Smith, 1995)	Cpx (Nimis, 1999)	Cpx (Putirka et al. 2003)	Two-pyroxene QUILF (Andersen et al. 1993)	Cpx (Putirka et al. 2003)	Hbl-Pl[a] (Holland and Blundy, 1994)	Zr-saturation (Watson and Harrison, 1983)	Ap-saturation (Harrison and Watson, 1984)
Main Intrusion	1.3 ± 0.4 ($n = 6$)					786 ± 36 ($n = 6$)	829 ± 11[b] ($n = 9$) 872 ± 4[c] ($n = 9$)	994 ± 2[b] ($n = 9$) 1091 ± 13[c] ($n = 9$)
Marginal Unit	1.1 ± 0.3 ($n = 11$)	5.5 ± 0.5[d] ($n = 6$) 4.4 ± 0.5[e] ($n = 4$)	5.5 ± 1[g] ($n = 4$) 1.1 ± 0.5[h] ($n = 7$)	1014 ± 21[d] ($n = 6$) 959 ± 10[e] ($n = 7$)	1094 ± 5[g] ($n = 4$) 1052 ± 10[h] ($n = 7$)	783 ± 40 ($n = 6$)	809 ± 5[b] ($n = 7$) 871 ± 4[c] ($n = 7$)	954 ± 12[b] ($n = 7$) 1108 ± 8[c] ($n = 7$)
CPM	0.8 ± 0.1 ($n = 2$)			874 ± 57 ($n = 5$)		797[f] ($n = 1$)	–	
MME	–			880 ± 5 ($n = 3$)		–	–	
Granitic seg.	1.9 ± 0.1 ($n = 4$)					748 ± 8 ($n = 2$)	910 ($n = 1$)	862 ($n = 1$)

[a] Using plagioclase rim composition of coexisting hornblende and plagioclase
[b] Bulk rock compositions were used
[c] Composition of granitic segregation was used
[d] Using core compositions of pyroxenes
[e] Using rim composition of pyroxenes
[f] Using coexisting hornblende and Na-rich plagioclase in complex plagioclase megacryst
[g] Maximum pressures and temperatures from Cpx-WR, incl. CPM and MME
[h] Minimum pressures and temperatures from Cpx-WR, incl. CPM

Results from the amphibole-plagioclase thermometer using hornblende and rim composition of coexisting plagioclase (oligoclase) suggest an average temperature of 785 ± 35 °C in the Main Intrusion and in the Marginal Unit, about 800 °C in the CPM and about 750 °C in the granitic segregations. Using the bulk chemistry, the method of zircon saturation in melts gives an average temperature of 829 ± 11 °C in the Main Intrusion, 809 ± 5 °C in the Marginal Unit (geochemical M-parameter of Watson and Harrison (1983) range 1.9 to 2.3) and ~910 °C in the granitic segregation. However, since rocks of both the Marginal Unit and Main Intrusion contain an appreciable amount of solid material that increases the M-parameter (mainly an effect of lowering the Si content), the saturation temperatures may be underestimated. Assuming that the composition of the granitic segregation (M-parameter = 1.52) represents a melt composition which approaches that present also within the other units, results in a average temperatures of 871 and 872 °C for the Marginal Unit and Main Intrusion, respectively (Table 6).

Calculated average saturation temperatures for apatite (after Harrison and Watson, 1984; Piccoli and Candela, 2002) are significantly higher than those for zircon, 954 and 994 °C for the Marginal Unit and Main Intrusion, respectively (Table 6). However, using the composition of the granitic segregation as an approximation of the melt composition (and that all P is dissolved in the melt) result in average saturation temperatures around 1100 °C.

It is important to note that there is no single crystallisation temperature for a plutonic rock since minerals are crystallizing over a considerable temperature interval. In our case, the clinopyroxene-liquid and two-pyroxene thermometers yielded the highest equilibrium temperatures (1015–1100 °C) estimating conditions closest to the liquidus for the Marginal Unit, whereas the amphibole-plagioclase temperature of the Main Intrusion, Marginal Unit, and granitic segregation (750–800 °C) represent conditions closer to the solidus (see Discussion).

Discussion

Evidence at variance with an origin by magma mixing, assimilation, or fractionation from a mafic precursor

In this section we argue against formation of the Vinga suite of rocks by: i) magma mixing, ii) assimilation or, iii) extensive crystal fractionation from a mafic parental magma. Instead, we will propose a model for crustal melting and an overlapping shift from unmixing to crystal fractionation to account for the evolution of the Vinga suite.

i) Assuming that the semi-contemporaneous late Sveconorwegian Göteborg dykes and the norites-monzonorites of the Hakefjorden complex represent possible variations in associated mafic magma compositions (in the absence of any suitable mafic rocks in the Vinga complex), the rocks of the Marginal Unit should form linear arrays between a specific mafic end member and the more felsic rocks of the Main Intrusion if magma mixing had occurred. This is not the case. Linear trends through the Marginal Unit extrapolate alternatively to the compositions of the Göteborg dykes, HFC-monzonorites or norites for different elements (Fig. 13).

Thus, no unique mafic end member can be defined. For example, the trends in the diagrams of Nb and Ni extrapolate to very primitive mafic end member compositions (more primitive than sampled in the HFC), whereas the Zr and TiO_2 trends extrapolate to Zr- and Ti-rich evolved compositions. Moreover, there is a distinct geochemical gap between the relatively homogeneous composition of the Marginal Unit and possible mafic end member compositions, rather than a continuous trend, which is expected from a magma mixing process. Similarly, the most mafic magmatic enclave does not consistently lie on a linear extension from the Vinga rocks, and hence, does not qualify as a mafic mixing end member. Although this geochemical evidence does not preclude the existence of an unknown mafic end member of the required composition, it does not favour such a model. Such an end member would have a composition at $SiO_2 =$ 50 wt% of approximately: $TiO_2 = 4\%$, $Al_2O_3 = 16\%$, $Fe_2O_3t = 13\%$, $MnO = 0.2\%$, $MgO = 5.5\%$, $CaO = 6\%$, $Na_2O = 3.5\%$, $K_2O = 2\%$, and P_2O_5 0.6%, Sum = 100.7%, with Ni = 120 ppm, Cr = 200 ppm, Rb = 25 ppm, Nb = 15 ppm, Zr = 500 ppm, Y = 25 ppm, Th = 2 ppm and Eu = 2 ppm. The major element compositon is similar to some ferrodiorites (e.g. Mitchell et al., 1996), but the high contents of Ni, Cr in combination with e.g. high Zr does not define a plausible mafic endmember.

Even though magmatic enclaves (chilled droplets of mafic-intermediate magmas) are numerous in the intrusion, and clearly suggest *mingling* of mafic to hybrid magmas with the Vinga rocks, the composition of these enclaves is completely different from that of the trend of the host rocks. The mafic enclaves appear to roughly form a separate trend of hybridization between a mafic end member, similar to the more evolved members of the HFC-norites and a felsic end member close to the composition of the Vinga Main Intrusion host (sketched in Fig. 13). However, with respect to the mafic end member the enclaves are enriched in K and particularly Rb; a feature that has been observed for many enclave suites and has been ascribed to selective enrichment through volatile transfer from the host granitoids and biotite formation (e.g. Bédard, 1990; Orsini et al., 1991; Stimac et al., 1995). Furthermore, field evidence for disaggregation of enclaves and associated hybridization with the host is lacking.

The abundance of non-igneous enclaves (quartz fragments, coarse feldspar-dominated enclaves, and gneissic xenoliths), showing evidence of disequilibrium and reaction with the magma, cannot be fitted into a model of mixing between two magmas. Rather, these represent partially melted crustal source material and/or partially assimilated wall rock contributions. The large and abundant CPMs in the Vinga rocks are a textural feature that is not easily accommodated in a model of magma mixing. Rapid growth of plagioclase in a mixed system should yield mainly euhedral, skeletal growth forms (e.g. Lofgren, 1974, 1980; Landi et al., 2004). It would theoretically be possible to obtain similar textural forms if the felsic magma just prior to the mixing event contained abundant large plagioclase crystals of a more albitic composition than that in equilibrium with the mixed magma, and if very extended plutonic re-equilibration times were available. However, in a mixed system, relatively fast overgrowth of new plagioclase of more anorthitic composition would tend to shield (e.g. Nakamura and Shimakita, 1998) and preserve the albite-rich parts in core areas (cf. e.g. Andersson and Eklund, 1994). The presence of identical CPMs in the coarse-grained feldspar-dominated enclaves support the argument that the CPMs did not form in a mixing system.

ii) In view of the large amounts of non-igneous enclaves in the Vinga magmas, dominantly quartz fragments, quartz ocelli, or quartzites that ubiquitously show reaction rims of amphibole, one would expect an important element of assimilation of metasedimentary rocks in the evolution of the magmas. However, the geochemical trends of the Vinga magmas lends no support for major assimilation, at least not of rocks similar to the local SLM metasediments (Fig. 13). Extension of the Vinga trends to high SiO_2 contents deviates substantially from the composition of the SLM metasediments for, e.g. Al_2O_3, MgO, K_2O, Rb, and Zr. In addition, the persistent metaluminous and alkali-calcic Vinga geochemistry is not in accordance with a major influence of assimilation of metasediments. Thus, these xenoliths and xenocrysts have been engulfed in the magma and partly reacted with it, but not assimilated extensively; all probably took place at the emplacement or subemplacement levels.

iii) Extended crystal fractionation from ferrodioritic (jotunitic) magmas has been advocated as the process for yielding the entire range of magma compositions in AMCG-complexes up to granite, supplemented by some crustal assimilation (e.g. Scoates et al., 1996; Duchesne and Wilmart, 1997; Frost et al., 2002; Bolle et al., 2003; Vander Auwera et al., 2003). The rocks of the Vinga Marginal Unit have higher or equally high abundances of Ni and Cr as the evolved rocks of the HFC (but lower MgO), as well as lower or equal amounts of, for example, Nb, Y, REE, Zr, and Ba (Figs. 13 and 14). This effectively precludes fractionation of ferromagnesian silicates from such parental magmas. Additionally, Na_2O, Al_2O_3, and Sr are higher in the Marginal Unit than in the more evolved HFC rocks, while CaO and Eu are lower. This does not allow a relation by plagioclase fractionation, and leaves only oxides and accessory minerals as possible fractionating phases. However, the decrease in CaO and MgO is not consistent with oxides dominating the fractionating assemblage, and no combination of accessory minerals can account for such trends. Another argument against the Vinga rocks evolving by extended fractionation from Fe-enriched jotunites is that this would lead to even stronger Fe-enrichment (e.g. Anderson et al., 2003; Scoates and Chamberlain, 2003). In contrast, the Vinga rocks and minerals are significantly less Fe-enriched compared with evolved, intermediate rocks from HFC (Fig. 12; Årebäck, 2001) and other AMCG-complexes (cf. e.g. Emslie and Stirling, 1993: Duchesne and Wilmart, 1997; Markl et al., 1998; Anderson et al., 2003). In addition, the development of CPMs, as those present in Vinga, have not been reported in extensively fractionated rocks from AMCG suites, nor is the texture expected to develop during normal fractional crystallization, but typical for environments of strong disequilibrium. However, crystal fractionation did occur within the Vinga magma following unmixing, but we argue that the former process is not the main mechanism for the origin of the Vinga parental magma.

Melting of metaluminous intermediate-granitic crustal sources

During melting of intermediate, metaluminous rock compositions, the liquidus temperatures are substantially higher in systems with low f_{H_2O} (e.g. Whitney, 1975; Johannes and Holtz, 1996), and the temperature interval between the solidus

and liquidus may exceed 300 °C (from <700 to >1000 °C; e.g. Wyllie, 1977). Water-saturated conditions are normally expected only at, or immediately above the solidus, giving way to increasing water dilution and undersaturation upon continued heating and melt formation (e.g. Johannes and Holtz, 1996). Among the felsic phases, plagioclase is normally the most refractory and quartz has typically the second highest thermal stability, particularly for calc-alkaline compositions (e.g. Conrad et al., 1988; Patiño Douce and Beard, 1995; Skjerlie and Johnston, 1996; Singh and Johannes, 1996). At pressures of the lower-middle crust, and temperatures above ca. 850–900 °C, experiments show that ortho- and/or clinopyroxene form at the expense of biotite and amphibole (and any minor garnet) as ferromagnesian silicates in partially molten granitoids of metaluminous, calc-alkaline to alkali-calcic compositions (e.g. Naney, 1983; Conrad et al., 1988; Skjerlie and Johnston, 1993, 1996; Patiño Douce and Beard, 1995; Singh and Johannes, 1996). This leaves a high-temperature assemblage of the major phases clinopyroxene + orthopyroxene + plagioclase ± Fe–Ti oxides ± quartz in equilibrium with a water-undersaturated melt, which is in agreement with the observed paragenesis and textural relations in the Marginal Unit of the Vinga intrusion (except for quartz). Such development during progressive heating of calc-alkaline crustal rocks has also been observed in natural examples (e.g. Bacon, 1992).

The temperature recorded by the clinopyroxene-liquid and two-pyroxene thermometry (>1000 °C) of compositions in the Marginal Unit (Table 6) supports the high-temperature nature of this magma. Such elevated temperatures in the crust result in a large proportion of anatectic melt (cf. Skjerlie and Johnston, 1996), leaving residual pyroxenes, plagioclase, and possibly some quartz to re-equilibrate. Hence, the pyroxenes are inferred to record a *minimum* estimate of the temperature conditions during melting in the source, as re-equilibration during slow cooling may have occurred in the source area before emplacement, and this is corroborated by the clinopyroxene barometry (mid-crustal depths). The lack of garnet and the HREE depletion in the Vinga rocks give additional support of a mid- rather than deep-crustal generation (<10 kbar; e.g. Patiño Douce and Beard, 1995; Singh and Johannes, 1996; Skjerlie and Johnston, 1996). Such elevated temperature conditions in the crust can only be attained as a result of an extra heat supply from the mantle, most probably in the form of mafic magma underplating or intraplating. Late Sveconorwegian mafic intrusions are well-known in the area (Årebäck, 2001; Hellström et al., 2004), as well as in SW Norway, where they are also associated with considerable amounts of mangerite to charnockite (e.g. Duchesne and Wilmart, 1997). Årebäck and Andersson (2002) estimated a mid-crustal intrusion level (4–6 kbar) for the Hakefjorden norite-anorthosite complex situated just 35 km to the north.

The relatively low temperatures (805–830 °C) calculated from the zircon saturation thermometry, together with the skeletal nature of the zircon crystals, indicate that the melt was undersaturated with respect to zircon at the elevated temperatures (>1000 °C) calculated for the Vinga magmas. A comparison with the experiments indicates that Zr contents need to be in excess of 2000 ppm for zircon to be saturated at 1000 °C for compositions such as those of the Vinga magmas. Moreover, using the composition of the the granitic segregation as an approximation of the *melt* composition also for the more mafic Vinga magmas results in appreciably higher saturation temperatures (ca. 870 °C), but still considerably lower than the

pyroxene temperatures. This demonstrates that all zircon was dissolved in melt at 1000 °C and that zircon present in a metaluminous source should become exhausted, which is supported by the very few identified inherited grains. This is in agreement with the model proposed by Miller et al. (2003) for the generation of 'hot', Zr-rich, but Zr-undersaturated granitoids. In addition, the relatively even Zr content (415–470 ppm) among the main Vinga rocks (except the late stage granitic segregations and dykes) is in accordance with complete solution and even distribution of Zr in the melt phase. The relatively high F contents in the Vinga magmas may have contributed to zircon dissolution during melting, but even higher contents are needed to affect zircon solubility (Keppler, 1993; Baker et al., 2002).

The metaluminous composition of all the Vinga rocks fulfils the criteria for the application of the apatite saturation thermometer of Harrison and Watson (1984). Assuming that the *melts* in the Vinga magmas had compositions somewhere between that of the Main Intrusion and granitic segregation suggests that apatite became saturated between 1000 and 1100 °C (Table 6), indicating that apatite may not have become entirely melted out of a metaluminous source.

Interpretation of the complex plagioclase megacrysts (CPMs)

During melting of crustal lithologies, plagioclase is a refractory phase (e.g. Johannes and Holtz, 1992, 1996, and references therein). Heating experiments and observations of natural partially melted quartzo-feldspathic rocks invariably show that plagioclase responds to elevated temperatures by partial dissolution/melting following crystallographically-oriented zones of weakness (e.g. Tsuchiyama and Takahashi, 1983; Tsuchiyama, 1985; Kaczor et al., 1988; Petcovic and Grunder, 2003). The crystals dissolve and new plagioclase with higher Ca-content, approaching the equilibrium composition at the elevated temperature of the system, begins to precipitate along the dissolution boundaries (e.g. Johannes, 1989; Johannes et al., 1994; Nakamura and Shimakita, 1998). Given enough time in a plutonic environment, heating to a temperature considerably above the solidus (but below the upper thermal stability of plagioclase), the entire original crystal may be completely replaced by a coarse, sieve-like, cellular grain, with a rounded irregular outline, whose composition is significantly enriched in the An-component.

We interpret the inner parts of the cells in the Vinga CPMs to represent plagioclase equilibrated at temperatures approaching the thermal maximum at the depth of magma generation. Only the most Ca-rich plagioclase and Mg-rich pyroxenes retain compositions approaching the thermal peak of the melting event (>1000 °C). Relatively stable conditions at elevated temperatures (e.g. during underplating) allowed for the slow dissolution of large protolith plagioclases and replacement by coarse Ca-enriched cellular grains (Fig. 10), and Na-enriched melt. The presence of identical plagioclases in the coarse, feldspar-dominated enclaves provides independent evidence for the formation of the CPMs by high-temperature dissolution as outlined above. This type of orthogranitoid enclave may in fact resemble the protolith lithology for the Vinga magmas, though presumably somewhat too felsic.

Årebäck and Andersson (2002) observed the presence of similar patchy, cellular-type plagioclases that formed in conjunction with partial melting in the contact aureole of the late Sveconorwegian HFC at metamorphic conditions of 890–

1015 °C and a pressure below 6 kbar. These cellular plagioclase grains are composed of a Ca-rich phase in the core, inferred to be in equilibrium during the high-temperature metamorphism and partial melting, and a more Na-rich phase at the rim that crystallized from the anatectic melt upon cooling. This textural evidence, suggests that complex plagioclase megacrysts can form during high-temperature melting of greywacke-type sediments as well, such as those of the SLM.

The preservation of well-developed plagioclase textures with their compositional zoning was made possible by the emplacement of the intrusion at essentially subvolcanic levels, 1–2 kbar as recorded by the Al-in-Hbl and Cpx-liquid barometry and miarolitic cavities. Slow cooling and re-precipitation of continuously more Na-rich plagioclase may, however, have started at depth. The drop in pressure and, in particular, the rapid cooling at the emplacement level resulted in the infilling of the CPMs as well as a rapid nucleation and growth of matrix plagioclase. Melt portions filling the voids in the sieve-like plagioclase crystallized as mafic minerals, quartz and K-feldspar. The composition of these mafic mineral inclusions is comparable to the rim composition of equivalent matrix minerals, suggesting that they were formed from the same melt. During emplacement, at relatively high temperatures, the Ca-rich rims began to develop around the CPMs, followed without interruption by the normal zoning of the rims and matrix plagioclase. The Na-enriched melt, trapped within the CPMs, also started to reprecipitate onto the Ca-enriched domains and continuously grew with normal zonation (Fig. 16). At this stage plagioclase commonly developed a boxy skeletal growth texture (Fig. 10; cf. Johannes et al., 1994; Hibbard, 1995; Nakamura and Shimakita, 1998).

Related magmatism

Other exposed late Sveconorwegian magmatic complexes in the nearby region are represented by the Iddefjord-Bohus granite complex (Eliasson et al., 2003), the Hakefjorden Complex (Årebäck, 2001), and the Göteborg dykes (Hellström et al., 2004) (Fig. 1). The latter two represent mafic magma input serving as potential heat sources for partial melting of the crust. In south Norway, the Rogaland Intrusive Complex contributed a major pulse of mafic magma input in late Sveconorwegian time (e.g. Schärer et al., 1996; Duchesne, 2001; Andersen and Griffin, 2004).

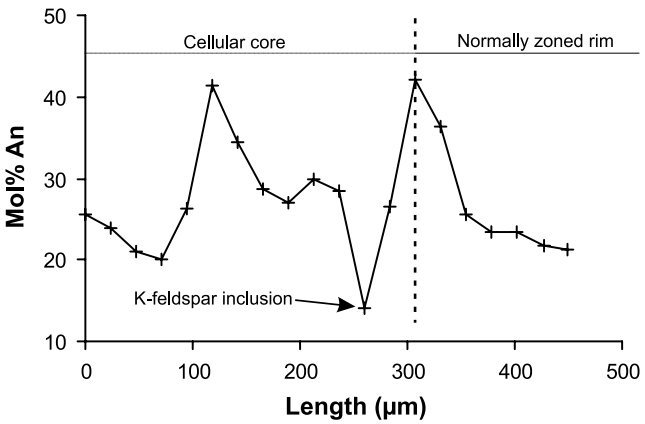

Fig. 16. Microprobe traverse through part of a CPM showing the variation in An-content. The variation of An-content in the cellular core is about the same as in the normally zoned rim. Sample 107. For traverse location see Fig. 11a

The Iddefjord-Bohus granite complex intruded mainly the metasediments of the Stora Le-Marstrand formation at 920 ± 5 Ma (Eliasson and Schöberg, 1991). It has imposed contact metamorphic assemblages that indicate an intrusive depth of about 15 km. A derivation from mixed ortho- and paragneisses during post-collisional extensional collapse has been proposed (Eliasson et al., 2003).

The Rogaland Intrusive Complex (RIC) is one of the best studied AMCG complexes worldwide (e.g. Duchesne, 2001). It crops out over an area of ca. 1750 km^2 and comprises major massif-type anorthosites, one large layered intrusion, major granitoid intrusions (granodiorite to charnockite) and numerous jotunitic to quartz mangeritic dykes (e.g. Duchesne, 2001, and references therein). It has been suggested that the jotunitic magmas (monzonorites) of RIC were derived from crustal sources by partial melting of basic rocks, coeval but not comagmatic with massif-type anorthosites (Duchesne et al., 1989; Bolle et al., 2003). According to Schärer et al. (1996) the RIC intruded the crust in a post-collisional setting at 932–920 Ma. However, recent data from zircons in the RIC indicate a crystallisation age of 949 ± 7 Ma, suggesting a duration of the magmatism from ca. 950 to 920 Ma (Andersen and Griffin, 2004). As in the case of many other massif-type anorthosite complexes, a polybaric crystallisation history has been inferred for RIC; from a deep seated magma chamber (at 11–13 kbar) up to mid-crustal depth ($\sim$5 kbar) (e.g. Duchesne et al., 1985; Longhi et al., 1999).

The 935 ± 3 Ma Göteborg dykes, east of Vinga, are a set of about 20 widely spaced WNW to W trending mafic dykes west of the Göta Älv Shear Zone in SW Sweden (Fig. 1; Hellström et al., 2004). Unlike the Vinga intrusion (and the HFC, described below) most of these dykes contain olivine (Hellström et al., 2004), which indicates that they are not as silica saturated as the former intrusions. The dykes are rich in Ti, K and P, and have a monzogabbroic composition. Hellström et al. (2004) proposed a common source-type for all the high Ti–K–P, mafic, late Sveconorwegian magmatic rocks in southern Scandinavia, including the RIC, HFC, and Göteborg dykes, although this can be questioned since the Göteborg dykes contain olivine.

The ca. 915 Ma Hakefjorden complex (HFC) is a Fe–Ti–P–K-rich norite-monzonorite intrusion (jotunitic), 5×1 km in size, with numerous blocks of anorthosite, trending W to WNW, (Fig. 1). The HFC, which shows similarities with Proterozoic massif-type anorthosites, has evolved through deep-crustal (high pressure) fractional crystallisation which produced anorthositic and ultramafic cumulates, followed by mid-crustal norite-monzonorite crystallisation; (Årebäck, 1995, 2001; Årebäck and Stigh, 1997, 2000).

Proposed petrogenetic model

Coarse, plagioclase-bearing source lithologies, presumably quartz monzonite to quartz monzodiorite (cf. starting compositions in the experiments of Patiño et al., 1995) of metaluminous, alkali-calcic composition at mid crustal depths (15–20 km) crust were underlain by hot, mantle-derived magmas, similar to other Sveconorwegian mafic intrusions (cf. Årebäck, 2001), in conjunction with the late Sveconorwegian post-collisional tectono-magmatic event (Fig. 17). The ponding of mafic magma caused the temperature rise to >1000 °C. At such elevated tem-

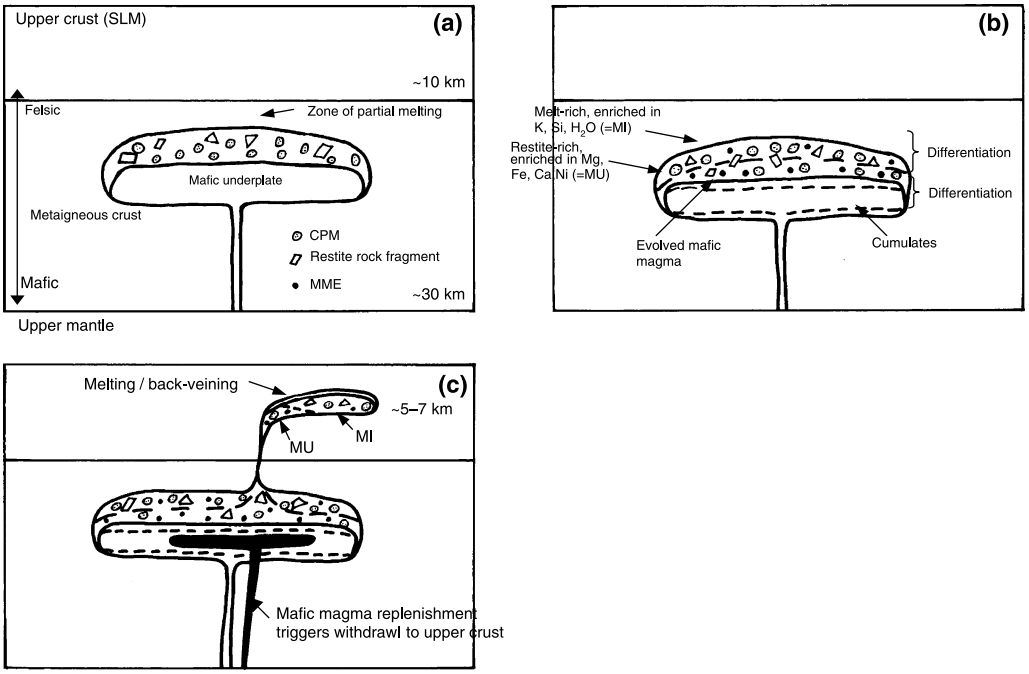

Fig. 17. Schematic sketch of the evolution of the Vinga intrusion. (**a**) A mafic, mantle-derived magma body, presumably similar to the HFC in composition, is emplaced at c. 20 km depth and induces melting of the crustal lithologies. The partially molten crustal rocks largely consist of alkali-rich, intermediate metaigneous rocks, containing relatively large plagioclase crystals. (**b**) The plagioclase develops into partially dissolved cellular megacrysts. Both the crustal and the mantle magmas differentiate into upper, more evolved and melt-enriched, and lower crystal-enriched layers. (**c**) Mingling of evolved mafic magma into the Vinga rocks as MMEs, and triggering of eruption to upper crustal levels, where textural and compositional features are preserved by rapid crystallization. Metasedimentary enclaves are engulfed and local melting results in aplitic back-veining of the intrusion. *MI* Main Intrusion, *MU* Marginal Unit

peratures the metaluminous source was extensively melted. Plagioclase, ortho- and clinopyroxene, and Fe–Ti oxides (±apatite) survived, while all other phases dissolved in the melt, including zircon. Bacon (1992) reported a similar case of crustal melting, however, at much shallower level, and postulated that in deeper melting zones the longer duration of heating would affect larger volumes and approach equilibrium. The large plagioclase crystals in the source rock began to dissolve, developing the cellular structure of the CPMs. The negative Eu anomaly for all rocks may indicate that some plagioclase should have remained in the source.

The composition of the Marginal Unit in comparison with the Main Intrusion represents a higher proportion of residual (restite) minerals in the former, and higher proportion of melt in the latter. Evidence for this is that the mineral phases that define the trends between the Marginal Unit and the Main Intrusion are those expected to remain residual or in equilibrium with a melt at $\geq$1000 °C at bulk compositions represented by the Vinga magmas, i.e. ortho- and clinopyroxene, Fe–Ti oxides, and minor plagioclase. The fractionation of these residual phases

('restite unmixing') is reflected by the steeply decreasing contents of MgO, Fe_2O_3, TiO_2, Ni, and less steep decrease of CaO, Sr, Na_2O, and steeply increasing Fe#, with increasing SiO_2 in the Harker diagrams (Fig. 13). The opposite trends for other elements reflect their partitioning into the melt phase.

At the composition of the most mafic rocks of the Main Intrusion a distinct inflection point, observable for most elements, marks the onset of a trend with different slope. This slope is less steep for particularly MgO, and Ni, reflecting the absence of orthopyroxene for this trend, while clinopyroxene and oxides persist. Steepened trends for CaO and Sr emphasize the increased importance of plagioclase removal. The shift to a slightly upward trend for Na_2O is most probably related to progressive partial melting of the CPMs, with the melt becoming enriched in Na and the residual plagioclase in Ca.

In the Main Intrusion, P_2O_5 and REE decrease with SiO_2, giving evidence for the beginning of crystallization and removal of apatite from the melt, which could have started already at temperatures >1000 °C according to the apatite saturation thermometry (Table 6). In contrast, Zr and Th increase, suggesting that the system was not saturated with zircon at this stage. Similarly, the increases of K_2O, Ba, and Rb show that K-feldspar and biotite are not part of the assemblage that is progressively removed from the magma. In fact, these components remain in the liquid until the latest stage, represented by the granitic segregation (Fig. 13). The composition of the late stage magma of the granitic segregation indicates separation of melt from a crystal mush consisting of clinopyroxene, plagioclase, Fe–Ti oxides, apatite, and probably amphibole (decreasing Nb, deepening Eu anomaly, middle REE most depleted, Figs. 13 and 14), but before major zircon crystallization as shown by the high Zr content (637 ppm).

In terms of processes, there is thus a shift from the 'unmixing' of unmelted (restite) phases early in the evolution, successively complemented and superseded by crystallization from the melt and fractionation of newly formed crystals and overgrowths on restite phases, and final separation of a residual liquid from a crystal mush. This sort of overlapping shift from unmixing to crystal fractionation may be much more common than previously recognized, particularly for crustal magmas.

Thus, we propose the following model for the evolution of the Vinga suite: the crustal magma started to differentiate at depth by the gravitational separation of residual solids (restite unmixing) into a lower portion (the Marginal Unit) being most enriched in solids, and an upper melt-enriched portion (the Main Intrusion) (Fig. 17). Concomitant with progressive melting of plagioclase, differentiation proceeded in the upper magma portion, at this stage involving also apatite crystallization from the melt, while zircon remained undersaturated. The melt became increasingly water-enriched and amphibole replaced clinopyroxene. The differentiation caused stratification with the melt- and fluid-enriched, lower-density parts on top. During withdrawal from the lower chamber the magmas preserved this general stratification and spread out laterally at the emplacement level as observed today (Fig. 17c).

The underplated mafic magma differentiated and the emplacement of the intrusion to upper crustal levels was triggered by the injection of a new pulse of mafic magma from below and/or tectonically induced pressure release. Relatively

evolved, Fe-rich portions of the uppermost layer of the underlying mafic magma were entrained and chilled (MME), partly mixed, in the Vinga magma as mafic-hybrid magmatic enclaves. The coarse, feldspar-dominated enclaves show signs of rejuvenation and partial melting from heating – corroded crystals, cellular dissolution and precipitation of melt as granophyric mesostasis in and around the corroded crystals. The CPMs distributed within the Vinga magmas originate from the disaggregation of such material. The gneissic and quartzitic enclaves and most of the quartz fragments represent more or less dissolved quartz-rich metasediments or quartz veins from the upper crust, presumably from lithologies equivalent to the surrounding SLM sedimentary formations (cf. Fig. 3a and b). This quartz-rich material was out of equilibrium, partly dissolved, and reacted with the intermediate Vinga magmas, developing reaction rims of amphibole (cf. Eklund and Lindberg, 1992).

During emplacement of the intrusion at subvolcanic levels (<7 km) the compositional differentiation was preserved as the intrusion spread out laterally and formed the Main Intrusion and the Marginal Unit. Rapid crystallization of plagioclase from the Na-enriched melt caused a continous normal zoning of the CPM cells and margins, as well as matrix plagioclases. The granophyric mesostasis, particularly developed around larger crystals (e.g. CPMs and quartz; Figs. 7c and 11) but also in the groundmass, is a result of rapid crystallization from the undercooled melt upon emplacement (cf. Candela, 1997). This also includes skeletal growth of accessory phases from the melt, most notably zircon.

As the Vinga magma crystallized early anhydrous phases, the H_2O content in the melt rose and amphibole replaced pyroxene in the crystallizing assemblage, together with biotite, particularly in the H_2O-richer Main Intrusion (Fig. 7b). The granitic segregations represent fluid-enriched late stage melt pockets. The aplitic dykes, on the other hand, have many geochemical characteristics in common with the SLM rocks (cf. Fig. 13), and are interpreted as melts formed in the metasedimentary country rocks due to the heat from the Vinga intrusion, and that backveined the intrusion at late stage. The crystallisation of the magma at this high crustal level is estimated from the clinopyroxene-liquid and amphibole-plagioclase thermometer (using plagioclase rim compositions) to have begun above 1000 °C and continued to at least 750 °C. The calculated temperatures and ubiquitous skeletal habit of zircon, apatite and pyrite clearly suggest crystallization upon rapid cooling during emplacement, when the melt became saturated in solidus or near-solidus phases below ca. 900 °C. This oversaturation and rapid growth of late stage phases during the emplacement may have been enhanced by saturation and loss of a vapour phase due to decompression (e.g. Lowenstern et al., 1997). Abundant miarolitic cavities throughout the intrusion, most common in the granitic segregations, support exsolution of a magmatic volatile phase, and the low pressures of emplacement (cf. Candela, 1997, and references therein).

Conclusions

1. The Vinga intrusion in SW Sweden comprises a suite of metaluminous, alkali-calcic, intermediate (55–63 wt% SiO_2) rocks. It contains a variety of enclaves, including mafic microgranular enclaves, coarse-grained feldspar-dominated

enclaves, quartz fragments and quartz-rich (gneissic) xenoliths of variable sizes. Granitic segregations represent late stage residual magmas.

2. The emplacement age was determined by U–Pb zircon SIMS geochronology to be 951 ± 7 Ma, overlapping within error with the previous U–Pb TIMS age of 963 ± 17 Ma (Åhäll and Schöberg, 1999). This shows that the Vinga intrusion belongs to an early pulse of late Sveconorwegian magmatism in SW Sweden (otherwise 935–915 Ma; Eliasson and Schöberg, 1991; Scherstén et al., 2000; Hellström et al., 2004), which is identical within error of the most recent U–Pb zircon dating of RIC (Andersen and Griffin, 2004).
3. The prominent porphyritic texture of the intrusion is dominated by large (<4 cm) irregularly rounded complex plagioclase megacrysts (CPMs). These consist of a coarse cellular network, where the cores of the cells are more calcic ($An_{50–35}$) compared with the margins ($An_{30–22}$). The outer rims of the CPMs and matrix plagiclase are normally zoned down to An_{22}. Identical CPMs occur in the coarse, feldspar-dominated enclaves. The CPMs are interpreted to result from high-temperature partial dissolution, compositional readjustment, and reprecipitation of original plagioclase grains from the protolith of the Vinga magma.
4. Pyroxene thermometry of the most mafic parts of the intrusion yielded temperatures in excess of 1000 °C, interpreted to reflect minimum temperatures of the source-melting event. Pressure conditions during melting, estimated from clinopyroxene compositions, are suggested to be mid-crustal, in the range 5–6 kbar. Hornblende-plagioclase thermometry on late stage amphibole and rim plagioclase yielded 750–800 °C, and Al-in-Hbl barometry ca. <2 kbar, corresponding to the high-level emplacement of the intrusion (<7 km). At 1000 °C, all Zr was dissolved in the melt, and crystallisation proceeded rapidly during emplacement below ca. 900 °C, as calculated from Zr saturation thermometry on skeletal zircon.
5. We propose that the magmas of the Vinga intrusion were generated from heating associated with intraplated, mafic, mantle-derived magma in the middle crust, from igneous, metaluminous, intermediate sources, containing abundant relatively large plagioclase crystals of oligoclase/andesine composition. As the temperature rose to >1000 °C, a major part of the source melted and only ortho- and clinopyroxene, plagioclase, and Fe–Ti oxides remained in the magma. Melt and solids differentiated gradually at depth, and the compositional stratification was preserved during emplacement. During emplacement, crystallisation resulted in normally zoned plagioclase and pyroxene crystals, biotite and amphibole precipitation, as well as rapid crystallisation of skeletal accessory minerals (zircon, pyrite and apatite) and granophyric mesostasis.
6. The following observations argue against alternative hypotheses: i) geochemical trends that are inconsistent with mixing and no identifiable mafic end member; ii) assimilation of metasediments does not explain the geochemical trends; iii) no reasonable fractionating assemblage can account for the geochemical transition from possible mafic parental magmas to the Vinga rocks; iv) the relatively low Fe-enrichment in the Vinga rocks and minerals, lower than in evolved rocks of spatially and temporally related mafic complexes; and v) the formation of large, rounded, cellular CPMs (by dissolution), and their presence in the coarse, feldspar-dominated enclaves.

Acknowledgements

We would like to thank the county administrative board of Västra Götaland for providing us with sampling authority at the conservation area of Vinga. Financial support by the Geological Survey of Sweden (SGU) contract No. 03–1102/2000 is gratefully acknowledged. Hans Harryson is thanked for technical assistance with the microprobe analyses at Uppsala University. Thanks also to Inger Lundqvist (SGU) for funding of five whole-rock analyses and to Anders Scherstén for providing a boat when we were mapping and sampling the small islands around Vinga. Thanks to T. Andersen, J. Scoates and C. Barnes for reviewing an earlier version of the manuscript. Journal reviews by Stefan Jung and an anonymous reviewer helped to improve the manuscript. The staff at NORDSIM is acknowledged. The NORDSIM facility is operated under an agreement between the research funding agencies of Denmark, Norway and Sweden, the Geological Survey of Finland, and the Swedish Museum of Natural History. This is NORDSIM contribution no. 134.

References

Åhäll K-I, Schöberg H (1999) The 963 Ma Vinga intrusion and post-compressional deformation in the Sveconorwegian orogen, SW Sweden. Geol Fören Stockholm Förh 121: 101–106

Åhäll K-I, Cornell DH, Armstrong R (1998) Ion probe dating of meta-sedimentary units across the Skagerrak: new constraints for early Mesoproterozoic growth of the Baltic Shield. Prec Res 87: 117–134

Altherr R, Henjes-Kunst F, Langer C, Otto J (1999) Interaction between crustal-derived felsic and mantle-derived mafic magmas in the Oberkirch pluton (European Variscides, Schwarzwald, Germany). Contrib Mineral Petrol 137: 304–322

Andersen T, Griffin WL (2004) Lu–Hf and U–Pb isotope systematics of zircons from the Storgangen intrusion, Rogaland Intrusive Complex, SW Norway: implications for the composition and evolution of Precambrian lower crust in the Baltic Shield. Lithos 73: 271–288

Andersen T, Andresen A, Sylvester AG (2002) Timing of late- to post-tectonic Sveconorwegian granitc magmatism in South Norway. Norges Geol Under Bull 440: 5–18

Anderson DJ, Lindsley DH, Davidson PM (1993) QUILF: a PASCAL program to assess equilibria among Fe–Mg–Mn–Ti oxides, pyroxenes, olivine, and quartz. Comput Geosci 19: 1333–1350

Anderson IC, Frost CD, Frost BR (2003) Petrogenesis of the Red Mountain pluton, Laramie anorthosite complex, Wyoming: implications for the origin of A-type granite. Prec Res 124: 243–267

Anderson JL, Smith DR (1995) The effects of temperature and fO_2 on the Al-in-hornblende barometer. Am Mineral 80: 549–559

Andersson UB, Eklund O (1994) Cellular plagioclase intergrowths as a result of crystal-magma mixing in the Proterozoic Åland rapakivi batholith, SW Finland. Contrib Mineral Petrol 117: 124–136

Årebäck H (1995) The Hakefjorden Complex – geology and petrogenesis of a late Sveconorwegian norite-anorthosite intrusion, south-west Sweden. Unpublished Ph.Lic. thesis, Earth Sciences Centre, Göteborg University A9

Årebäck H (2001) Petrography, geochemistry and geochronology of mafic to intermediate late Sveconorwegian intrusions: the Hakefjorden Complex and Vinga intrusion, SW Sweden. Unpublished Ph.D. thesis, Earth Sciences Centre, Göteborg University A72

Årebäck H, Stigh J (1997) Polybaric evolution of the Hakefjorden complex, southwestern Sweden, deduced from partial dissolution in andesine megacrysts. Geol Fören Stockholm Förh 119: 97–101

Årebäck H, Stigh J (2000) Nature and origin of an anorthosite associated ilmenite-rich leuconorite, Hakefjorden complex, SW Sweden. Lithos 51: 247–267

Årebäck H, Andersson UB (2002) Granulite-facies contact metamorphism around the Hakefjorden norite-anorthosite complex, SW Sweden. N Geol Tids 82: 29–44

Bacon CR (1992) Partially melted granodiorite and related rocks ejected from Crater Lake caldera, Oregon. Trans Roy Soc Edinburgh Earth Sci 83: 27–47

Baker DH, Conte AM, Freda C, Ottolinei L (2002) The effect of halogens on Zr diffusion and zircon dissolution in hydrous metaluminous granitic melts. Contrib Mineral Petrol 142: 666–678

Barbarin B (1990) Plagioclase xenocrysts and mafic magmatic enclaves in some granitoids of the Sierra Nevada batholith, California. J Geophys Res 95: 17747–17756

Bateman R (1995) The interplay between crystallization, replenishment and hybridization in large felsic magma chambers. Earth Sci Rev 39: 91–106

Bédard J (1990) Enclaves from the A-type granite of the Mégantic complex, White Mountain magma series: clues to granite magma genesis. J Geophys Res 95: 17797–17819

Blake DH, Elwell RWD, Gibson IL, Skelhorn RR, Walker GPL (1965) Some relationships resulting from the intimate association of acid and basic magmas. Quart J Geol Soc London 121: 31–49

Bolle O, Demaiffe D, Duchesne J-C (2003) Petrogenesis of jotunitic and acidic members of an AMC suite (Rogaland anorthosite province, SW Norway): a Sr and Nd isotopic assessment. Prec Res 124: 185–214

Candela PA (1997) A review of shallow, ore-related granites: texture, volatiles, and ore metals. J Petrol 38: 1619–1633

Chappell BW, White JR, Wyborn D (1987) The importance of residual source material (resite) in granite petrogenesis. J Petrol 28: 1111–1138

Chen YD, Price RC, White AJR, Chappell BW (1990) Mafic inclusions from the Glenbog and Blue Gum granite suites, southeastern Australia. J Geophys Res 95: 17757–17785

Collins WJ, Richards SR, Healy BE, Ellison PI (2000) Origin of heterogeneous mafic enclaves by two-stage hybridisation in magma conduits (dykes) below and in granitic magma chambers. Trans Roy Soc Edinburgh Earth Sci 91: 27–45

Connely JN, Åhäll K-I (1996) The Mesoproterozoic cratonization of Baltica; new constraints from SW Sweden. In: Brewer TS (ed) Precambrian crustal evolution in the North Atlantic Regions. Geol Soc Publ 112: 261–273

Conrad WK, Nicholls IA, Wall VJ (1988) Water-saturated and undersaturated melting of metaluminous to peraluminous crustal compositions at 10 kb: evidence for the origin of silicic magmas in the Taupo volcanic zone, New Zealand, and other occurrences. J Petrol 29: 765–803

Duchesne JC (ed) (2001) The Rogaland intrusive massifs – an excursion guide. NGU report 2001. 029. Geological Survey Norway

Duchesne JC, Wilmart E (1997) Igneous charnokites and related rocks from the Bjerkreim-Sokndal layered intrusion (Southwest Norway): a jotunite (hypersthene monzodiorite)-derived A-type granitoid suite. J Petrol 38: 337–369

Duchesne JC, Maquil R, Demaiffe D (1985) The Rogaland anorthosites: facts and speculations. In: Tobi AC, Touret JLR (eds) The deep Proterozoic crust in the north Atlantic provinces. D. Reidel, Dordrecht, pp 449–476

Duchesne JC, Wilmart E, Demaiffe D, Hertogen J (1989) Monzonorites from Rogaland (Southwest Norway): a series of rocks coeval but not comagmatic with massif-type anorthosites. Prec Res 45: 111–128

Eklund O, Lindberg B (1992) Interaction between basaltic melts and their wallrock in dykes and sills in Åland, southwestern Finland. Geol Fören Stockholm Förh 114: 93–102

Eklund O, Fröjdö S, Lindberg B (1994) Magma mixing, the petrogenetic link between anorthositic suites and rapakivi granites, Åland, SW Finland. Mineral Petrol 50: 3–19

Eliasson T, Schöberg H (1991) U–Pb dating of the post-kinematic Sveconorwegian (Grenvillian) Bohus granite, SW Sweden: evidence of restitic zircon. Prec Res 51: 337–350

Eliasson T, Ahlin S, Petersson J (2003) Emplacement mechanism and thermobarometry of the Sveconorwegian Bohus granite, SW Sweden. Geol Fören Stockholm Förhan 125: 113–130

Emslie RF (1978) Anorthosite massifs, rapakivi granites, and late Proterozoic rifting in North America. Prec Res 7: 61–98

Emslie RF (1991) Granitoids of rapakivi granite-anorthosite and related association. Prec Res 51: 173–192

Emslie RF, Hunt PA (1990) Ages and petrogenetic significance of igneous mangerite-charnockite suites associated with massif anorthosites, Grenville Province. J Geol 98: 213–231

Emslie RF, Stirling JAR (1993) Rapakivi and related granitoids of the Nain plutonic suite: Geochemistry, mineral assemblages and fluid equilibria. Can Mineral 31: 821–847

Emslie RF, Hamilton MA, Thériault RJ (1994) Petrogenesis of a mid-proterozioc anorthosite-mangerite-charnockite-granite (AMCG) complex: isotopic and chemical evidence from the Nain plutonic suite. J Geol 102: 539–558

Frost BR, Barnes CG, Collins WJ, Arculus RJ, Ellis DJ, Frost CD (2001) A geochemical classification for granitic rocks. J Petrol 42: 2033–2048

Frost CD, Frost BR, Bell JM, Chamberlain KR (2002) The relationship between A-type granites and residual magmas from anorthosite: evidence from the northern Sherman batholith, Laramie Mountains, Wyoming, USA. Prec Res 119: 45–71

Frost TP, Mahood GA (1987) Field, chemical, and physical constraints on mafic-felsic magma interaction in the Lamarck Granodiorite, Sierra Nevada, California. Geol Soc Am Bull 99: 272–291

Halsor SP, Rose WI (1991) Mineralogical relations and magma mixing in calc-alkaline andesites from Lake Atitlán, Guatemala. Mineral Petrol 45: 47–67

Harrison TM, Watson EB (1984) The behaviour of apatite during crustal anatexis: equilibrium and kinetic considerations. Geochim Cosmochim Acta 48: 1467–1477

Hattori K, Sato H (1996) Magma evolution recorded in plagioclase zoning in 1991 Pinatubo eruption products. Am Mineral 81: 982–994

Hellström F, Johansson Å, Larsson SÅ (2004) Age and emplacement of late Sveconorwegian monzogabbroic dykes, SW Sweden. Prec Res 128: 39–55

Hibbard MJ (1981) The magma mixing origin of mantled feldspar. Contrib Mineral Petrol 76: 158–170

Hibbard MJ (1995) Petrography to petrogenesis. Prentice-Hall, Englewood Cliffs

Holland T, Blundy J (1994) Non-ideal interactions in calcic amphiboles and their bearing on amphibole-plagioclase thermometry. Contrib Mineral Petrol 116: 433–447

Hraško L, Kotov AB, Salnikova EB, Kovach VP (1998) Enclaves in the Rochovce granite intrusion as indicators of the temperature and origin of the magma. Geol Carpathica 49: 125–138

Johannes W (1989) Melting of plagioclase-quartz assemblages at 2 kbar water pressure. Contrib Mineral Petrol 103: 270–276

Johannes W, Koepke J, Behrens H (1994) Partial melting reactions of plagioclase and plagioclase-bearing systems. In: Parson I (ed) Feldspars and their reactions. Kluwer Academic Publishers, pp 161–194

Johannes W, Holtz F (1992) Melting of plagioclase in granite and related systems: composition of coexisting phases and kinetic observations. Trans Roy Soc Edinburgh Earth Sci 83: 417–422

Johannes W, Holtz F (1996) Petrogenesis and experimental petrology of granitic rocks. Springer, Berlin

Johansson F (1997) Petrology and geochemistry of Neoproterozoic WNW trending dolerite dykes in the Göteborg Region, SW Sweden. Unpublished M.Sc. thesis, Earth Sciences Centre, Göteborg University B60

Kaczor SM, Hanson GN, Peterman ZE (1988) Disequilibrium melting of granite at the contact with a basic plug: a geochemical and petrographic study. J Geol 96: 61–78

Keppler H (1993) Influence of fluorine on the enrichment of high field strength elements in granitic rocks. Contrib Mineral Petrol 114: 479–488

Kolker A, Lindsley DH (1989) Geochemical evolution of the Maloin Ranch pluton, Laramie anorthosite complex, Wyoming: petrology and mixing relations. Am Mineral 74: 307–324

Kuo LC, Kirkpatrick RJ (1982) Pre-eruption history of phyric basalts from DSDP legs 45 and 46: evidence from morphology and zoning patterns in plagioclase. Contrib Mineral Petrol 79: 13–27

Landi P, Métrich N, Bertagnini A, Rosi M (2004) Dynamics of magma mixing and degassing recorded in plagioclase at Stromboli (Aeolian Archipelago, Italy). Contrib Mineral Petrol 147: 213–227

Larsen LL, Smith EI (1990) Mafic enclaves in the Wilson Range pluton, northwestern Arizona: implications for the generation of a calc-alkaline intermediate pluton in an extensional environment. J Geophys Res 95: 17693–17716

Lindberg B, Eklund O (1988) Interactions between basaltic and granitic magmas in a Svecofennian postorogenic granitoid intrusion, Åland, southwest Finland. Lithos 22: 13–23

Lofgren G (1974) An experimental study of plagioclase crystal morphology: isothermal crystallization. Am J Sci 274: 243–273

Lofgren G (1980) Experimental studies on the dynamic crystallization of silicate melts. In: Hargraves RB (ed) Physics of magmatic Processes. Princeton University Press, pp 487–551

Longhi J, Vander Auwera J, Fram MS, Duchesne JC (1999) Some phase equilibrium constraints on the origin of Proterozoic (Massif) anorthosites and related rocks. J Petrol 40: 339–362

Lowenstern JB, Clynne MA, Bullen TD (1997) Comagmatic A-type granophyre and rhyolite from the Alid Volcanic Center, Eritrea, northeastern Africa. J Petrol 38: 1707–1721

Ludwig KR (1998) On the treatment of concordant uranium-lead ages. Geochim Cosmochim Acta 62: 665–676

Lundegårdh PH (1953) Petrology of the Möndal-Styrsö-Vallda region in the vicinity of Gothenburg. SGU C 531

Lundqvist I (2000) Bedrock map of Göteborg municipality, scale 1:50000. SGU Ba 59

Markl G (2001) REE constraints on fractionation processes of massive-type anorthosites on the Lofoten Islands, Norway. Mineral Petrol 72: 325–351

Markl G, Frost BR, Bucher K (1998) The origin of anorthosites and related rocks from the Lofoten island, northern Norway: I. Field relations and estimation of intrinsic variables. J Petrol 39: 1425–1452

Miller CF, McDowell SM, Mapes RW (2003) Hot and cold granites? Implications of zircon saturation temperatures and preservation of inheritance. Geology 31: 529–532

Mitchell JN, Scoates JS, Frost CD, Kolker A (1996) The geochemical evolution of anorthosite residual magmas in the Laramie anorthosite complex, Wyoming. J Petrol 37: 637–660

Müller A, Seltmann R (2002) Plagioclase-mantled K-feldspar in the Carboniferous porphyritic microgranite of Altenberg-Frauenstein, eastern Erzgebirge/Krušné Hory. Bull Geol Soc Finland 74: 53–78

Nakamura M, Shimakita S (1998) Dissolution origin and syn-entrapment compositional change of melt inclusion in plagioclase. Earth Planet Sci Lett 161: 119–133

Naney MT (1983) Phase equilibria of rock-forming ferromagnesian silicates in granitic systems. Am Mineral 283: 993–1033

Nelson ST, Montana A (1992) Sieve-textured plagioclase in volcanic rocks produced by rapid decompression. Am Mineral 77: 1242–1249

Nimis P (1999) Clinopyroxene geobarometry of magmatic rocks. Part 2. Structural geobarometers for basic to acidic, tholeiitic and mildy alkaline magmatic systems. Contrib Mineral Petrol 135: 62–74

Orsini J-B, Cocirta C, Zorpi M-J (1991) Genesis of mafic microgranular enclaves through differentiation of basic magmas, mingling and chemical exchanges with their host granitoid magmas. In: Dider J, Barbarin B (eds) Enclaves and granite petrology. Developments in petrology. Elsevier, Amsterdam, pp 445–464

Patiño Douce A, Beard JS (1995) Dehydration melting of biotite gneiss and quartz amphibolite from 3 to 15 kbar. J Petrol 36: 707–738

Petcovic HL, Grunder AL (2003) Textural and thermal history of partial melting in tonalitic wallrock at the margin of a basalt dike, Wallowa Mountains, Oregon. J Petrol 44: 2287–2312

Piccoli PM, Candela PA (2002) Apatite in igneous systems. In: Kohn MJ, Rakovan J, Hughes JM (eds) Phosphates, geochemical, geobiological, and materials importance, Rev Mineral Geochem 48: Mineral Soc Am, pp 255–292

Poli G, Tommasini S (1991) Model for the origin and significance of microgranular enclaves in calc-alkaline granitoids. J Petrol 32: 657–666

Putirka KD (1999) Clinopyroxene + liquid equilibria to 100 kbar and 2450 K. Contrib Mineral Petrol 135: 151–163

Putirka KD, Mikaelian H, Ryerson F, Shaw H (2003) New clinopyroxene-liquid thermobarometers for mafic, evolved, and volatile-bearing lava compositions, with applications to lavas from Tibet and the Snake River Plain, Idaho. Am Mineral 88: 1542–1554

Rämö OT, Haapala I (1995) One hundred years of rapakivi granite. Mineral Petrol 52: 129–185

Ratajeski K, Glazner AF, Miller BV (2001) Geology and geochemistry of mafic to felsic plutonic rocks in the Cretaceous intrusive suite of Yosemite Valley, California. Geol Soc Am Bull 113: 1486–1502

Reid JB Jr, Evans OC, Fates DG (1983) Magma mixing in granitic rocks of the central Sierra Nevada, California. Earth Planet Sci Lett 66: 243–261

Romer RL, Smeds SA (1996) U–Pb columbite ages of pegmatites from Sveconorwegian terranes in southwestern Sweden. Prec Res 76: 15–30

Sallet R (2000) Fluorine as a tool in the petrogenesis of quartz-bearing magmatic associations: applications of an improved F–OH biotite-apatite thermometer grid. Lithos 50: 241–253

Sandeman HAI, Clark AH, Scott DJ, Malpas JG (2000) The Kennack gneiss of the Lizard Peninsula, Cornwall, SW England: commingling and mixing of mafic and felsic magmas accompanying Givetian continental incorporation of the Lizard ophiolite. J Geol Soc London 157: 1227–1242

Schärer U, Wilmart E, Duchesne JC (1996) The short duration and anorogenic character of anorthosite magmatism: U–Pb dating of the Rogaland complex, Norway. Earth Planet Sci Lett 139: 335–350

Scherstén A, Årebäck H, Cornell DH, Hoskin P, Åberg A, Armstrong R (2000) Dating mafic-ultramafic intrusions by ion-probing contact-melt zircon: examples from SW Sweden. Contrib Mineral Petrol 139: 115–125

Scoates JS, Chamberlain KR (2003) Geochronologic, geochemical and isotopic constraints on the origin of monzonitic and related rocks in the Laramie anorthosite complex, Wyoming, USA. Prec Res 124: 269–304

Scoates JS, Frost CD, Mitchell JN, Lindsley DH, Frost BR (1996) Residual liquid origin for a monzonitic intrusion in a mid-Proterozoic anorthosite complex: the Sybille intrusion, Laramie anorthosite complex, Wyoming. Geol Soc Am Bull 108: 1357–1371

Singer BS, Pearce TH, Kolisnik AM, Myers JD (1993) Plagioclase zoning in mid-Pleistocene lavas from the Seguam volcanic center, central Aleutian arc, Alaska. Am Mineral 78: 143–157

Singh J, Johannes W (1996) Dehydration melting of tonalites. Part II. Composition of melts and solids. Contrib Mineral Petrol 125: 26–44

Skjerlie KP, Johnston AD (1993) Fluid-absent melting behavior of an F-rich tonalitic gneiss at mid-crustal pressures: implications for the generation of anorogenic magmas. J Petrol 34: 785–815

Skjerlie KP, Johnston AD (1996) Vapour-absent melting from 10 to 20 kbar of crustal rocks that contain multiple hydrous phases: implications for anatexis in the deep to very deep continental crust and active continental margins. J Petrol 37: 661–691

Stacy JS, Kramers JD (1975) Approximation of terrestrial lead isotope evolution by a two-stage model. Earth Planet Sci Lett 36: 207–221

Stewart ML, Fowler AD (2001) The nature and occurrence of discrete zoning in plagioclase from recently erupted andesitic volcanic rocks, Montserrat. J Volcan Geother Res 106: 243–253

Stewart ML, Pearce TH (2004) Sieve-textured plagioclase in dacitic magma: interference imaging results. Am Mineral 89: 348–351

Stimac JA, Clark AH, Chen Y, Garcia S (1995) Enclaves and their bearing on the origin of the Cornubian batholith, southwest England. Mineral Mag 59: 273–296

Streckeisen A (1976) To each plutonic rock its proper name. Earth Sci Rev 12: 1–33

Taylor SR, McLennan SM (1985) The continental crust: its composition and evolution. Blackwell, Oxford

Tindle AG, Webb PC (1994) PROBE-AMPH – a spreadsheet program to classify microprobe-derived amphibole analyses. Comput Geosci 20: 1201–1228

Tsuchiyama A (1985) Dissolution kinetics of plagioclase in the melt of the system diopside-albite-anorthite, and origin of dusty plagioclase in andesites. Contrib Mineral Petrol 89: 1–16

Tsuchiyama A, Takahashi E (1983) Melting kinetics of plagioclase feldspar. Contrib Mineral Petrol 84: 345–354

Vance JA (1965) Zoning in igneous plagioclase: patchy zoning. J Geol 73: 636–651

Vander Auwera J, Bogaerts M, Liégeois J-P, Demaiffe D, Wilmart E, Bolle O, Duchesne J-C (2003) Derivation of the 1.0–0.9 Ga ferro-potassic A-type granitoids of southern Norway by extreme differentiation from basic magmas. Prec Res 124: 107–148

Vernon RH (1984) Microgranitoid enclaves in granites – globules of hybrid magma quenched in a plutonic environment. Nature 309: 438–439

Vernon RH (1990) Crystallization and hybridism in microgranitoid enclave magmas: microstructural evidence. J Geophys Res 95: 17849–17859

Wager LR, Bailey EB (1953) Basic magma chilled against acid magma. Nature 172: 68–69
Walker GPL, Skelhorn RR (1966) Some associations of acid and basic igneous rocks. Earth Sci Rev 2: 93–109
Watson EB, Harrison TM (1983) Zircon saturation revisited: temperature and composition effects in a variety of crustal magma types. Earth Planet Sci Lett 64: 295–304
Whalen JB, Currie KL (1984) The Topsails igneous terrane, western New Foundland: Evidence for magma-mixing. Contrib Mineral Petrol 87: 319–327
Whalen JB, Currie KL, Chappel BE (1987) A-type granites: geochemical characteristics, discrimination and petrogenesis. Contrib Mineral Petrol 95: 407–419
White AJR, Chappell BW (1977) Ultrametamorphism and granitoid genesis. Teconophysics 43: 7–22
Whitehouse MJ, Claesson S, Sunde T, Vestin J (1997) Ion microprobe U–Pb zircon geochronology of Archaean gneisses from the Lewisian Complex of Gruinard Bay, northwestern Scotland. Geochim Cosmochim Acta 61: 4429–4438
Whitehouse MJ, Kamber B, Moorbath S (1999) Age significance of U–Th–Pb zircon data from early Archean rocks of west Greenland – a reassessment based on combined ion-microprobe and imaging studies. Chem Geol 160: 201–224
Whitney JA (1975) The effects of pressure, temperature, and X_{H_2O} on phase assemblage in four synthetic rock compositions. J Geol 83: 1–31
Wiebe RA (1980) Comingling of contrasted magmas in the plutonic environment: examples from the Nain anorthositic complex. J Geol 88: 197–209
Wiedenbeck M, Allé P, Corfu F, Griffin WL, Meier M, Oberli F, von Quadt A, Roddick JC, Spiegel W (1995) Three natural zircon standards for U–Th–Pb, Lu–Hf, trace element and REE analysis. Geostand Newslett 19: 1–23
Wyllie PJ (1977) Crustal anatexis: an experimental review. Tectonophysics 43: 41–71
Wyllie PJ, Cox KG, Biggar GM (1962) The habit of apatite in synthetic systems and igneous rocks. J Petrol 3: 238–243
Zeck HP (1992) Restite-melt and mafic-felsic magma mixing and mingling in an S-type dacite, Cerro del Hoyazo, southeastern Spain. Trans Roy Soc Edinburgh Earth Sci 83: 139–144